Modelling the Failure of Reinforced Concrete Subjected to Dynamic Loading Using CDPM2 in LS-DYNA

Eleanor Lockhart

Year 5
MEng in Civil Engineering with Architecture
ENG5295P

ABSTRACT

It is important to understand the effects of dynamic loading, such as blast or fragment impact, on building materials to avoid structural failure and subsequent disaster. The response of concrete subjected to blast loading can be analysed by constitutive models which predict the response of concrete subjected to multiaxial compression. Concrete Damage Plasticity Model 2 (CDPM2) is a constitutive model which uses plasticity and damage mechanics to describe multiaxial stress states. It has been implemented in the finite element program LS-DYNA.

Previous University of Glasgow studies have investigated the suitability of CDPM2 for modelling plain concrete structures subjected to dynamic loading. However, in practice structural concrete is almost always reinforced in some way. Therefore, assessing whether CDPM2 is suitable for modelling reinforced concrete is an important step in proving CDPM2 to be a reliable tool for use in the analysis of concrete structures subjected to dynamic loading.

In this project, a number of different models are analysed in order to verify and validate CDPM2 for modelling the response of reinforced concrete structures to dynamic loading. Mesh-independency is investigated using models with different mesh sizes and comparisons are made between the results of a physical experiment and the response of the model of this experiment.

CONTENTS

LIST OF SYMBOLS

Roman Uppercase Letters

A	cross-sectional area of steel reinforcing bar
A_h	hardening ductility parameter in CDPM2
A_s	ductility parameter during damage in CDPM2
B_h	hardening ductility parameter in CDPM2
B_s	damage ductility exponent during damage in CDPM2
C	strain rate parameter in MAT_PLASTIC_KINEMATIC material model for steel
C_h	hardening ductility parameter in CDPM2
D_f	flow rule parameter in CDPM2
D_h	hardening ductility parameter in CDPM2
E	Young's modulus
E_c	Young's modulus of concrete
E_t	tangent modulus of steel
E_s	Young's modulus of steel
F_{co}	rate dependent parameter in CDPM2
F_y	force at which yielding occurs in steel
G_F	fracture energy of concrete
H_p	hardening parameter in CDPM2
L	length
N	axial load applied to tension member
N_c	force in concrete at a point along the length of a tension member
N_s	force in steel at a point along the length of a tension member
$\bar{N}_c$	average force in concrete over the length of a tension member
$N_{c,max}$	maximum force in concrete between cracks in a tension member
$\bar{N}_s$	average force in steel over the length of a tension member
P	strain rate parameter in MAT_PLASTIC_KINEMATIC material model for steel
P_{cr}	tensile capacity of tension member

Roman Lowercase Letters

c	speed of sound
$c_{3D-continuum}$	speed of sound through a 3D-continuum in LS-DYNA
c_{beam}	speed of sound though a beam element in LS-DYNA
e	eccentricity parameter in CDPM2

f_c	ultimate compressive strength of concrete
f_{ci}	compressive stress at which the initial yield surface is reached in concrete
f_s	effective plastic strain for eroding elements in MAT_PLASTIC_KINEMATIC material model for steel
f_t	ultimate tensile strength of concrete
f_{t1}	tensile strength threshold value for bi-linear damage formulation in CDPM2
h	element size of model
l	length
m_g	dilation variable in CDPM2
q_{h0}	initial hardening modulus in CDPM2
q_{h1}, q_{h2}	hardening variables in CDPM2
s	slip of concrete relative to reinforcement
s_1	slip at maximum bond stress
t	time
v_p	formulation for rate effects in MAT_PLASTIC_KINEMATIC material model for steel
w_f	tensile threshold value for linear tensile damage formulation in CDPM2
w_{f1}	tensile threshold value for the second part of the bi-linear damage formulation in CDPM2
w_u	ultimate crack width of concrete subjected to tension
w_c	crack width of concrete subjected to tension
x_s	ductility measure in CDPM2

Greek Letters

α_ϵ	coefficient to account for changes in the Young's modulus of concrete for different types of aggregate
α_r	strain rate factor in CDPM2
β	hardening parameter in MAT_PLASTIC_KINEMATIC material model for steel
δ_e	elastic displacement
δ_y	displacement at which yielding occurs in steel
Δ	change in value, used as prefix
ε_0	threshold strain of concrete for initiation of damage in CDPM2
ε_{fc}	parameter controlling compressive damage softening branch
ε_c	elastic strain of concrete subjected to compression

ε_t	elastic strain of concrete subjected to tension
ε_{wc}	crack strain
$\bar{\theta}$	Lode angle
κ_p	hardening variable in CDPM2
ρ	density
$\bar{\rho}$	deviatoric effective stress
ρ_c	density of concrete
ρ_s	density of steel
σ	nominal stress tensor
$\bar{\sigma}$	effective stress tensor
σ_c	axial tensile stress
$\bar{\sigma}_c$	negative part of the effective stress tensor
σ_y	yield stress of steel
$\bar{\sigma}_t$	positive part of the effective stress tensor
τ	bond stress
τ_{max}	maximum bond stress
υ	Poisson's ratio
υ_c	Poisson's ratio of concrete
υ_s	Poisson's ratio of steel
ω_c	compressive damage variable in CDPM2
ω_t	tensile damage variable in CDPM2

PREFACE

In this project, a number of different models are analysed in order to verify and validate CDPM2 for modelling the response of reinforced concrete structures to dynamic loading.

The work was carried out between September 2016 and January 2017 to satisfy the requirements of the final year individual project as part of the Civil Engineering with Architecture MEng degree programme. The project was undertaken in the School of Engineering at the University of Glasgow.

I would like to thank my supervisor, Dr Peter Grassl, for his continued support and guidance throughout the project, my family for their support, and all other contributors to the project.

1 INTRODUCTION

1.1 Background

Blast and fragment impact on buildings, caused by man-made or natural hazards, are examples of severe dynamic loading which can have disastrous effects, such as building collapse and loss of life, if the structure is not designed to resist sufficiently. Therefore, it is important to understand the effects of such loading on the building materials used in the structure.

Full-scale tests on building materials can be carried out but these can be costly, time consuming and dangerous to operators. They also may not be practical on very small or very large scales. The use of computer modelling is a more economical and safer way to gain an understanding of the response of materials, provided the model used has been demonstrated to be sufficiently accurate in predicting the material's behaviour.

The response of concrete subjected to blast loading can be analysed by constitutive models which predict the response of concrete subjected to multiaxial compression. Concrete Damage Plasticity Model 2 (CDPM2) is a constitutive model which uses plasticity and damage mechanics to describe multiaxial stress states. It has been implemented in the finite element program LS-DYNA.

Previous University of Glasgow projects have shown that CDPM2 can be used in LS-DYNA to accurately predict the maximum load capacity of a concrete beam subjected to bending (McTaggart, 2016) and the local tensile behaviour of a small concrete sample subjected to high-strain rate loading (Fraser, 2016). Both of these studies examined plain concrete. However, in practice, structural concrete is almost always reinforced in some way. Therefore, assessing whether CDPM2 is suitable for modelling reinforced concrete is an important step in proving CDPM2 to be a reliable tool for use in the analysis of concrete structures subjected to dynamic loading.

1.2 Aims and Objectives

This project aims to evaluate the suitability of CDPM2 for modelling the response of reinforced concrete structures to dynamic loading.

The objectives of the project are:

- To investigate the modelling of reinforced concrete using CDPM2 in LS-DYNA.

- To verify and validate CDPM2 for modelling reinforced concrete, where verification is the process of checking that the results of the model agree with mathematical theory and validation is the process of checking the level of accuracy with which the model reproduces the same results as those obtained in physical experiments.
- To improve understanding of the behaviour of reinforced concrete subjected to dynamic loading by modelling a particular method of providing blast resistance i.e. fibre-reinforcement.

1.3 Project Outline

Chapter 2 provides a literature review of the concepts involved in the project including the verification and validation processes, the behaviour of reinforced concrete, and some background and theory behind CDPM2.

Chapter 3 provides information about the modelling of reinforced concrete, including descriptions of the CDPM2 input parameters, methods of modelling the bond between reinforcement and concrete, and the determination of time-step used in LS-DYNA analyses.

Chapter 4 presents the analyses of a number of different models, and discusses the results obtained. Firstly, a single element is analysed to gain an understanding of LS-DYNA analysis results and to investigate the effects of changing element size. Secondly, prisms subjected to tension are modelled with different mesh sizes, with and without reinforcement, to verify mesh independency and investigate the methods of modelling reinforcement. A physical experiment is then described and modelled, and comparisons made between the results. Fibre-reinforcement is then modelled and the results also compared to the physical experiment. Finally, changes are made to the relationship between the concrete and reinforcement and the effects discussed. Input files from analyses are given as appendices.

Chapter 5 concludes the report with a summary of the project findings and suggestions for future research.

2 LITERATURE REVIEW

This section describes the concepts involved in the project including the verification and validation processes, the behaviour of reinforced concrete and some background and theory behind CDPM2. It aims to inform the reader of the purpose of the project, explain some of the terms used, and provide information on the reasons for the development of CDPM2 and how it works.

2.1 Verification and Validation

Schaller (2004) explains that when computer models are developed, their correctness and accuracy must be checked before they can be used to make engineering predictions. Verification and validation (V&V) are processes which allow the accuracy of model predictions and their level of agreement with physical experiments to be measured. They are used to measure whether a model is sufficiently correct and accurate for its specific intended use rather than for all possible scenarios.

According to Schaller (2004), the process of verification confirms that the model produces results which agree, with sufficient accuracy, with the mathematical theory surrounding that which is being modelled. It can be divided into code verification and calculation verification. Code verification is used to check that the software being used is working as anticipated and that the user is operating it correctly (software quality assurance), and that the model can return results which match analytical solutions (numerical algorithm verification). Calculation verification is used to determine the level of uncertainty in the numerical simulation by considering, for example, whether convergence is reached with mesh refinement. Mesh dependency is investigated in this project.

Validation is described by Schaller (2004) as a process which assesses the level of agreement between the results produced by a model and corresponding physical experiment(s). There can be errors and uncertainties in both the model and the physical experiments, so it is important to note that validation can only confirm if there is sufficient accuracy for the particular use which has been modelled and physically tested.

2.2 Reinforced Concrete Behaviour

It is well-known that concrete behaves differently when under tension and compression. It is much stronger in compression than tension. Its ultimate tensile strength can be as little as 5-10% of its compressive strength (Chen, 2007). In construction, it is common for reinforcement

bars to be placed in the areas of concrete under tension, to allow the full compressive capacity of the concrete to be used, while the reinforcement resists in tension. Therefore, it is important to understand the material behaviours when modelling reinforced concrete.

2.2.1 Concrete

Failure of concrete is defined in Chen (2007) as loss of strength in both tension and compression, with the development of major cracks perpendicular to load direction in tension.

The main ingredients of concrete are cement, water and aggregate. Chen (2007) explains that before any load is applied, concrete already has many microcracks existing in it. This can be due to segregation of the ingredients, shrinkage, or thermal expansion. They can also form once loading has begun because of the differing stiffnesses of the aggregate and cement. The interfaces between the aggregates and the cement are where the microcracks tend to form because these are the weakest areas of the concrete. The propagation of these cracks when concrete is loaded contributes to the non-linear load-displacement response, and causes an increase in volume near the point of failure.

The low tensile strength of concrete is primarily due to the weakness of the aggregate-cement interface in tension. Figure 2.1(a) (Nesset and Skoglund, 2017: 15) shows the stress-strain curve for concrete subjected to tension (or low-confined compression).

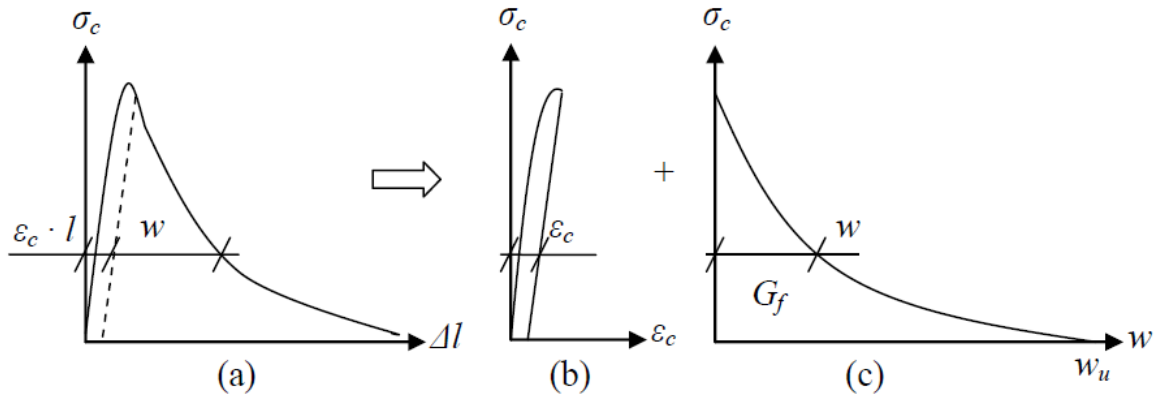

Figure 2.1 Stress-strain curve for concrete subjected to tension (or low-confined compression) (Nesset and Skoglund, 2017: 15).

When it is uniaxially loaded in tension, initially it will behave elastically, as seen in Figure 2.1(b). According to Chen (2007), when stress reaches around 60% of the tensile strength f_t, microcracks in a localised zone start to grow because stress concentrations develop at their tips. Once the stress exceeds around 75% f_t some of the cracks bridge together and reach their critical length. After the tensile strength is exceeded, the concrete will demonstrate strain-softening: the reduction of stress with increasing strain, seen in Figure 2.1(c). Stress will continue to decrease as cracks widen until no more tensile stress can be

transmitted across the cracks. Figure 2.1 demonstrates how the overall displacement Δl in Figure 2.1(a) of a specimen of concrete is related to both the elastic displacement ε_c in Figure 2.1(b) and the ultimate crack-opening w_u in Figure 2.1(c).

The amount of energy required to create a crack of unit surface area projected in a plane parallel to the crack direction is called fracture energy, G_F (Hillerborg et al.,1976: 773-781). It is released as forms of energy such as heat and sound when a crack forms and is equal to the area under the stress-strain curve.

The cracks that form in tension are perpendicular to the direction of loading rather than parallel to it, meaning the area available to carry the load decreases as loading is increased (Chen, 2007).

In compression, Chen (2007) states that microcracks start to propagate at only 30% of the compressive strength f_c when behaviour becomes non-linear. Cracks will bridge together at between 50% and 75% of f_c, reaching their final lengths at around 75% f_c. Strain-softening will then occur but failure is much more brittle than in tension. There is no clear stress crack-opening: instead failure is caused by lots of small cracks rather than a few long cracks. Concrete is a quasi-brittle material, which means that strain hardening is followed by tension softening after the ultimate tensile strength is reached (Bhushan, 2010) Although it is a quasi-brittle failure, it is at a much higher stress, due in part to the development of friction between the cracks. Under increasing confinement, the compressive strength significantly increases and the concrete becomes more ductile (Chen, 2007).

Cracks propagate in the direction parallel to loading. This causes the phenomenon known as dilation: when concrete is compressed under low confinement, although its volume initially decreases, at a certain stage of loading it will undergo a volumetric expansion.

2.2.2 Reinforcement

Steel is used as reinforcing bars to resist tensile forces in the concrete. Steel is ductile and when subjected to tensile loading it initially exhibits a linear elastic stress-strain relationship with a gradient equal to its Young's modulus, up to an elastic limit. The stress at this point is called the yield strength. After this, discontinuities in the force-displacement relationship can occur depending on the strength of the steel. However, it is usually acceptable to represent the relationship as shown in Figure 2.2 (Williams, 2012: 2.1).

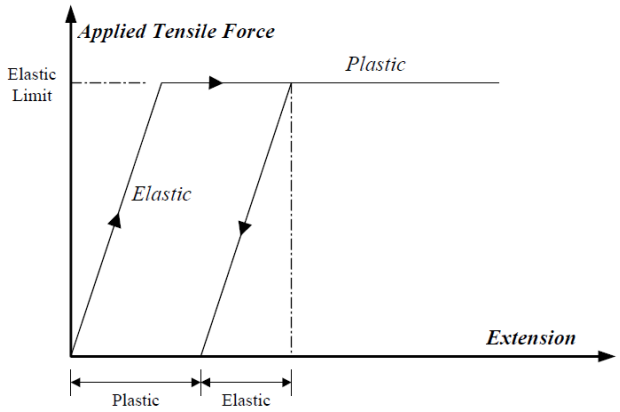

Figure 2.2 Force-displacement graph for steel subjected to tension (Williams, 2012: 2.1).

2.2.3 Bond Between Concrete and Reinforcement

The response of reinforced concrete depends not only on the behaviour of the individual materials but on the interaction between them. Forces in the reinforcing bars are transferred to the concrete through 'bond stresses' τ at the interface between the two materials. These are shear stresses acting parallel to the reinforcement. The transfer of forces can cause discrepancies between the forces in the two materials, along with the formation of cracks in the concrete, this causes relative displacement between the reinforcing bars and the concrete. This displacement is called "slip".

The relationship between bond and slip can be affected by many factors including, but not limited to: bar size and roughness (bars can be ribbed or smooth); concrete cover; and position and orientation of the bars during casting of the concrete (CEB-FIP, 1990: 82).

2.2.4 Tension Stiffening

Bischoff (2001) states that before cracking of reinforced concrete subjected to tension, the concrete and steel reinforcement share the applied load in proportion to their rigidities. Stresses and strains are uniform along the length of the member. When the concrete cracks, the stress in the steel at the locations of the cracks increases significantly, discontinuing the uniformity of stress along the member length. At the crack locations, only the steel carries the tensile stresses. Between the cracks, the tension is still carried by both the steel and the concrete, through transfer of the forces in the bond between the two materials. Tension stiffening is the result of the tension in the concrete. It effectively reduces the strain in the steel and allows more force to be carried by reinforced concrete members compared to a bare reinforcing bar on its own (bare steel). Figure 2.3 (modified from Bischoff, 2001: 364) demonstrates the increase in tensile capacity of a reinforced member compared to the response of bare steel.

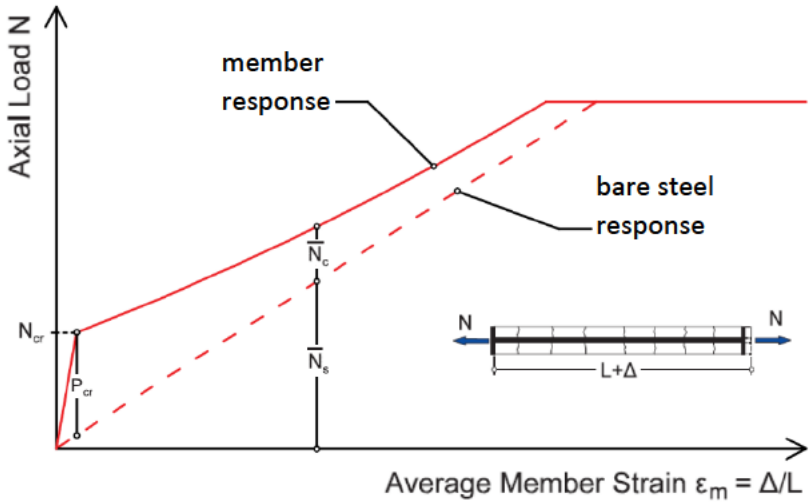

Figure 2.3 Force-strain graph for reinforced concrete member subjected to tension (modified from Bischoff, 2001: 364).

Figure 2.4 (modified from Bischoff, 2001: 365) shows the non-uniform distribution of load N along the length of a cracked member. N_c and N_s represent the force in the concrete and steel at a point along the length of the member, respectively. $\overline{N}_c$ and $\overline{N}_s$ represent the average forces in the concrete and steel over the whole length of the member, respectively. The force in the steel at crack locations is N_{sb}. The force in the concrete varies parabolically between each crack, from zero at the cracks up to a maximum $N_{c,max}$. If this maximum exceeds the tensile capacity P_{cr} then another crack will form at this location. In order for $N_{c,max}$ to reach P_{cr}, there must be sufficient distance between cracks. This distance must be twice the bond transfer length i.e. the distance from a crack face required for P_{cr} to develop. When crack spacing becomes too small, no more cracks will form in the concrete. It should be noted that cracks are often not spaced regularly as Figure 2.4 might imply. Although the minimum spacing is required to form new cracks, they are most often very randomly spaced.

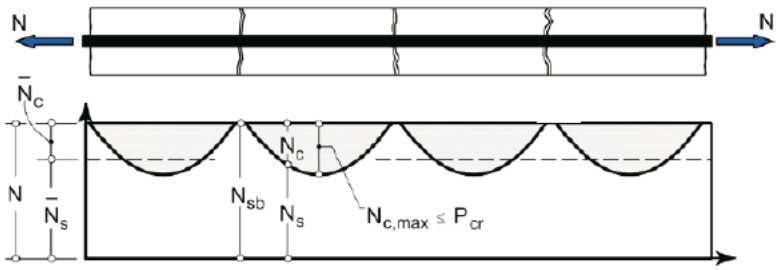

Figure 2.4 Load distribution along the length of a cracked reinforced concrete member (modified from Bischoff, 2001: 365).

Tension stiffening can be affected by various factors including the compressive strength of the concrete and shrinkage of the concrete.

2.2.5 Shrinkage

While concrete to be used in an experiment is curing, it tends to shrink slightly, even if it is cured in a moist environment (Bischoff, 2001). The amount of shrinkage increases with increasing concrete strength (Fields and Bischoff, 2004). When reinforced concrete is the subject of the experiment, this shrinkage causes an initial shortening of the whole member, before any load is applied to it. Fields and Bischoff (2004) explain that this produces compressive stresses in the reinforcement and initial tension in the concrete. These initial tensile stresses lead to the formation of cracks at a lower load, giving an apparent reduction in the load required to produce the first crack.

Omitting the effects of shrinkage when analysing experimental results can produce a lower post-cracking strength (tension stiffening) then should be obtained, and the extent of this reduction can appear to be dependent on reinforcing ratio and size of shrinkage strain, which is not the case (Bischoff, 2001). It is therefore important to include the effects of shrinkage to evaluate tension stiffening effects properly.

Although shrinkage can affect tension stiffening significantly, it does not influence cracking to the same extent, according to Bischoff (2001). This is because the measurement of crack widths (strains) in experiments takes account of shrinkage strains even when they are not intentionally considered.

2.3 CDPM2 Background and Theory

Concrete Damage Plasticity Model 2 (CDPM2) is a constitutive material model which has been implemented in the finite element program LS-DYNA. It uses plasticity and damage mechanics to describe multiaxial stress states, to allow the analysis of concrete subjected to dynamic loading (Grassl et al., 2013). It is a development of its original model, CDPM1.

Grassl et al. (2013) explain that before the development of CDPM1, both stress-based plasticity models and strain-based damage mechanics models, and combinations of these had been developed but none were capable of describing completely the failure of concrete. Plasticity models are useful for modelling some aspects of the failure, like deformations in confined compression, but cannot describe the reduction of stiffness that occurs during unloading of the concrete when softening takes place. Damage mechanics models can describe other aspects such as this stiffness degradation, but are restricted to tensile and low confined compressive stress states. Correctly combining the two models allows a more realistic representation of concrete failure.

Like CDPM2, CDPM1 combined plasticity and damage mechanics. Grassl et al. (2013) state that the model agreed well with physical experiments. It provided results which were independent of the size of the mesh (mesh-independent). However, the damage part was based on a single parameter to represent both tension and compression which did not allow the transition between tensile and compressive failure to be realistically described.

The major improvement in CDPM2 is that it can describe the transition from tension to compression more realistically than CDPM1 because it introduces two separate damage variables for tension and compression.

CDPM2 is based on the following stress-strain relationship:

$$\sigma = (1 - \omega_t)\bar{\sigma}_t + (1 - \omega_c)\bar{\sigma}_c \tag{2.1}$$

where σ is the nominal stress tensor, $\bar{\sigma}_t$ and $\bar{\sigma}_c$ are the positive and negative parts of the effective stress tensor $\bar{\sigma}$, respectively, and ω_t and ω_c are the tensile and compressive damage variables respectively, which range from 0 (undamaged) to 1 (fully damaged). The plastic part of the model determines the effective stress tensor and the damage part determines the damage variables. An outline of the process by which (2.1) is calculated, as given by Grassl et al. (2013) is given below.

The plastic part, represented by Figure 2.1(b), uses the given strain increment to evaluate trial values of the principle effective stresses (and their directions) which are then converted to the Haigh-Westergaard co-ordinates. These consist of the volumetric effective stress $\bar{\sigma}_c$, the norm of the deviatoric effective stress $\bar{\rho}$ and the Lode angle $\bar{\theta}$. Along with the hardening variables, κ_p, q_{h1} and q_{h2} and an elliptic function $r(cos(\bar{\theta})$, these co-ordinates describe the cylindrical yield surface of the concrete. The true principle stresses are then determined and separated into the tensile and compressive parts.

The calculation of the rate of plastic strain is not associated with the yield function i.e. the flow rule is non-associated. This means the direction of plastic flow is not normal to the yield surface. The flow rule is determined using the fact that, in the softening regime, concrete in uniaxial tension will produce elastic strains perpendicular to load direction and in compression will undergo a volumetric expansion. It involves a dilation variable m_g which controls the ratio of volumetric and deviatoric plastic flow.

Damage is initiated when the elastic strain (equivalent strain) in the concrete reaches the threshold strain of $\varepsilon_0 = \frac{f_t}{E_c}$ (where f_t is the tensile strength and E_c is the Young's modulus of the concrete). After this, damage, e.g. cracks, will start to form as described in section 2.2.1.

The damage part of the constitutive model allows the strain due to cracking, represented by Figure 1(c), to be included in the overall strain of the concrete.

The maximum equivalent strain in the history of loading the concrete is determined from the yield surface in a way which is suitable for both tension and compression. The damage parameters are determined from the damage history variables, which are different for tension and compression, using a ductility measure x_s and strain rate factor α_r. This allows a relationship between stress and damage to be obtained.

Damage in tension is represented by a relationship between stress σ_t and crack width w (converted from inelastic tensile strain ε_t by multiplying by element length h) for which there are three options: linear, bilinear and exponential. The bilinear relationship is shown in Figure 2.5(a) (Grassl, 2016). Damage in compression is represented by an exponential relationship between stress and inelastic strain ε_c, as shown in Figure 2.5(b). The parameters w_f, w_{f1}, f_t, f_{t1}, A_s and ε_{fc} are input parameters described in section 3.1.1.

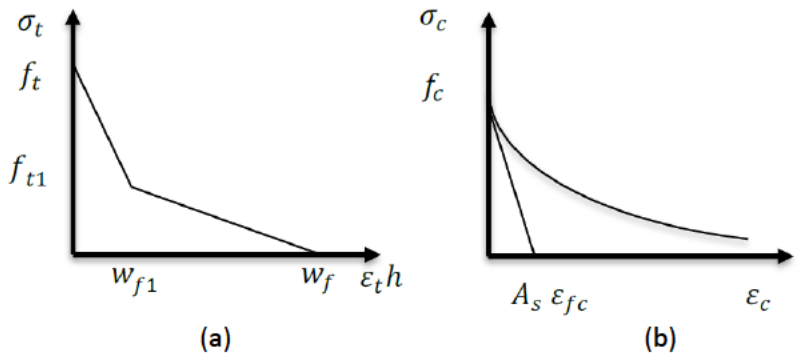

Figure 2.5 Stress-crack strain relationships used in CDPM2 for (a) tension (b) compression (Grassl, 2016).

3 MODEL

3.1 Constitutive Models

The models in this report use the CDPM2 material model (MAT_CDPM) for concrete and the MAT_PLASTIC_KINEMATIC material for reinforcement. The material model input parameters are described in this section.

3.1.1 Constitutive Model for Concrete

The twenty-three input parameters in the CDPM2 material model card used in LS-DYNA are described below, as explained in Grassl (2016). The description of the input refers to the parameters in LS-DYNA. They are mostly related to physical properties which can be determined from tests such as uniaxial compressive and tensile tests, and three-point bend tests, or appropriate expressions. The parameters are:

- **Density, ρ_c**: mass density of the concrete, taken as 2300 kg/m^3 for all analyses in this project, as CEB-FIP (2010) gives the range for normal weight concrete as 2000-2600 kg/m^3;
- **Young's modulus, E_c**: modulus of elasticity which gives a measure of the stiffness of the concrete. When E_c is unknown, the following relationship from CEB-FIP (2010) can be used:

$$E_c = 21.5\alpha_\epsilon \left(\frac{f_c}{10}\right)^{1/3} \tag{3.1}$$

  where f_c is the compressive strength of the concrete, and α_ϵ is a coefficient to account for changes in the Young's modulus of concrete for different types of aggregate. A value of 1.0 is used in this project, assuming quartzite aggregate for simplicity, although other types of aggregate would require different α_ϵ values;

- **Poisson's ratio, υ_c**: gives the degree to which the concrete will deform in directions lateral to the direction of loading, taken as 0.2 for all analyses in this project, as given in Bright and Roberts (2010) for uncracked concrete;
- **Eccentricity parameter, *e***: automatically calculated from Jirásek and Bazant (2002) as:

$$ECC = \frac{1+\epsilon}{2-\epsilon}, \qquad \epsilon = \frac{f_t(f_{bc}^2 - f_c^2)}{f_{bc}(f_c^2 - f_t^2)}, \qquad f_{bc} = 1.16 f_c \qquad \text{3.2(a), (b), (c)}$$

- **Initial hardening modulus, q_{h0}**: equal to f_{ci}/f_c where f_{ci} is the compressive stress at which the initial yield surface is reached. The default is 0.3;
- **Uniaxial tensile strength of the concrete, f_t**;

- **Uniaxial compressive strength of the concrete, f_c**;
- **Hardening parameter, H_p**: the default is 0.5, but a value of 0.01 is recommended when the application does not involve strain rate effect if a realistic description of the transition from tension to compression is important, so 0.01 is used for all analyses in this project;
- **Hardening ductility parameters, A_h, B_h, C_h and D_h**: the defaults are 0.08, 0.003, 2.0, and $1x10^{-6}$ respectively;
- **Ductility parameter during damage, A_s**: the default is 15;
- **Damage ductility exponent during damage, B_s**: the default is 1;
- **Flow rule parameter, D_f**: describes dilation. The default is 0.85;
- **Rate dependent parameter, F_{c0}**: only required if strain rate dependency is considered, for which 10 MPa is the recommended value;
- **Tensile damage type**: Damage in tension is represented by a relationship between stress and crack width for which there are three options: linear, bilinear and exponential. Input can be 0 = linear, 1 = bilinear, 2 = exponential or 3 = no damage. The default is linear but bilinear is recommended for best results and is shown in Figure 2.5(a);
- **Tensile threshold value for linear tensile damage formulation, w_f**: represents the crack width at which no more stress is transferred between the two pieces of concrete on either side of the crack, as shown in Figure 2.5(a). It can be obtained from the fracture energy of the concrete. The fracture energy is equal to the area under the graph, which gives rise to the following formula if the bilinear relationship is used:

$$w_f = 4.444 \times \frac{G_F}{f_t} \tag{3.3}$$

  where G_F = fracture energy, f_t = tensile strength and w_{f1} and f_{t1} are left as default. Grassl (2016) recommends scaling the value of w_f by 0.56 to account for an overestimation of fracture energy which occurs when tetrahedral elements are used, because of the way the element length is determined. Where the fracture energy is unknown, the following relationship from [CEB-FIP 2010] can be used:

$$G_F = 73 f_c^{0.18} \tag{3.4}$$

  where f_c is the compressive strength of the concrete;

- **Tensile threshold value for the second part of the bi-linear damage formulation, w_{f1}**: as shown in Figure 2.5(a). The default is $0.15w_f$;
- **Tensile strength threshold value for bi-linear damage formulation, f_{t1}**: as shown in Figure 2.5(a). The default is $0.3f_t$;
- **Strain rate flag**: turns strain rate effects on or off, where 0 = off, 1 = on;

- **Failure flag**: turns erosion (elements with zero stiffness are deleted) on or off, where 0 = off, and a value other than zero gives the percentage of integration points which must fail before erosion is executed;
- **Parameter controlling compressive damage softening branch,** ε_{fc}: in the exponential compressive damage formulation as shown in Figure 2.5(b). The smaller the value, the more brittle the failure. The default is $1x10^{-4}$ m.

3.1.2 Constitutive Model for Reinforcement

The nine input parameters in the MAT_PLASTIC_KINEMATIC material model card used in LS-DYNA are described below, as explained in Livermore Software Technology Corporation (2016a). The description of the input refers to the parameters in LS-DYNA. They are mostly related to physical properties which can be determined from tests. The parameters are:

- **Density,** ρ_s: mass density of the steel, taken as 7850 kg/m^3 for all analyses in this project;
- **Young's modulus,** E_s: modulus of elasticity which gives a measure of the stiffness of the steel, taken as 200 GPa for the single element and prism tests in sections 4.1 and 4.2 respectively, as assumed in Bright and Roberts (2010);
- **Poisson's ratio,** υ_s: gives the degree to which the steel will deform in directions lateral to the direction of loading, taken as 0.3 for all analyses in this project, as given in Bright and Roberts (2010);
- **Yield stress,** σ_y: the stress at which the steel will yield, taken as 500 MPa for the single element and prism tests in sections 4.1 and 4.2 respectively, as assumed in Bright and Roberts (2010);
- **Tangent modulus,** E_t: the slope of the bilinear stress-strain curve of the steel after yielding. The default is 0;
- **Hardening parameter,** β: used to combine kinematic and isotropic hardening and varies between 0 = kinematic (default) and 1 = isotropic;
- **Strain rate parameters, P and C**: for Cowper Symonds strain rate model, which scales the yield stress according to these parameters and the strain rate. The default for both is 0 which means strain rate effects are ignored;
- **Effective plastic strain for eroding elements,** f_s: The default is $1x10^{20}$;
- **Formulation for rate effects,** v_p: when strain rate effects are considered, this determines whether the yield stress is scaled (0, default) or a viscoplastic formulation is applied (1).

3.1.3 Constitutive Model for Bond Between Reinforcement and Concrete

The CONSTRAINED_BEAM_IN_SOLID keyword was used to give the bond-slip relationship (see sections 2.2.3 and 3.2). The input parameters are described as follows, as explained in (Livermore Software Technology Corporation, 2016b):

- **Slave**: used to indicate the part or part set ID of the reinforcing beam;
- **Master**: used to indicate the part or part set ID of the concrete;
- **Coupling direction**: The default is 0 which applies the constraint along all directions, whereas 1 applies the constraint along only directions normal to the beam, so no constraint is applied in the beam axial direction;
- **Start and end times for coupling**: The default for both is 0;
- **ID of a user defined function which describes the bond-slip relationship**: 0 turns the function off (used in the perfect bond cases in this project), -n means that a function with ID equal to n is used (used in the bond-slip cases in this project). See Appendix 2 for how the relationship was written.

3.2 Techniques to Model Reinforcement and its Interaction with Concrete

Three methods of modelling the reinforced concrete were used: two methods which represent perfect bond between the reinforcement and the concrete and one which represents bond-slip.

3.2.1 Shared Nodes

Perfect bond was modelled firstly with shared nodes where the nodes of the concrete were part of the same mesh as the reinforcement, as denoted in Figure 3.1. Further information about this method can be found in Schwer (2014).

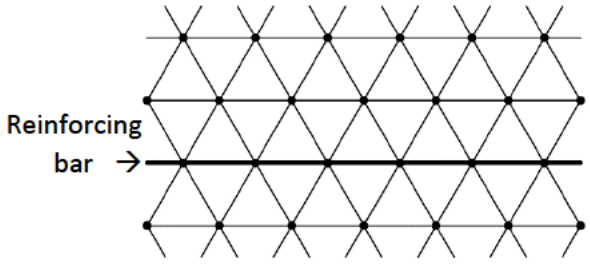

Figure 3.1 Tetrahedral mesh with shared nodes.

3.2.2 Constrained without Bond-slip

Perfect bond was modelled secondly with constrained nodes using the keyword CONSTRAINED_BEAM_IN_SOLID, where the meshes of the two materials were modelled separately and superimposed, but the displacement between the nodes of each material was constrained to zero. Figure 3.2 represents constrained nodes. Further information about this method can be found in Schwer (2014).

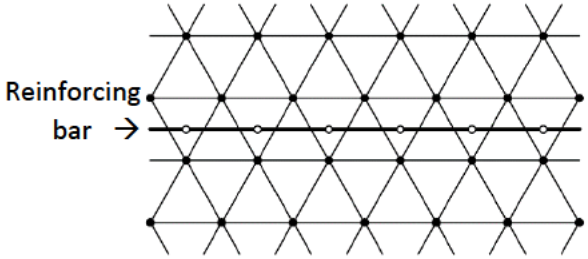

Figure 3.2 Tetrahedral mesh with constrained nodes.

3.2.3 Constrained with Bond-slip

For the case with bond-slip, the constrained nodes method was used but with a relationship to control the displacement (slip) between the concrete and the reinforcement. CEB-FIP (1990) recommends the relationship between bond-stress and slip (bond-slip) shown in Figure 3.3.

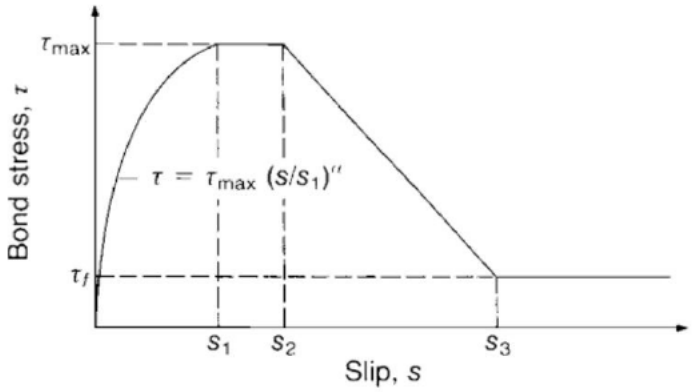

Figure 3.3 Relationship between bond-stress and slip (CEB-FIP, 1990).

However, slip is not usually expected to increase to much more than s_1 so the relationship is simplified in analyses in this study to that shown in Figure 3.4, where the maximum bond stress, $\tau_{max} = 2\sqrt{(f_c - 8)}$ and a value for s_1 of 0.6 mm is recommended for unconfined concrete.

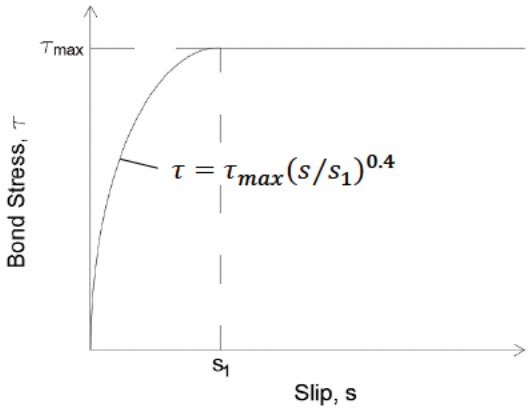

Figure 3.4 Simplified bond-slip relationship used in this study.

Another method for modelling the bond-slip could be to use the shared nodes approach but to apply 'springs' to separate the nodes of each material. The stiffness of the springs reflects the strength of the bond between concrete and reinforcement. This method was considered too complex for the nature of this project and so was not adopted. More information can be found in Nesset and Skoglund (2007) where this method has been used.

3.3 Time Step

LS-DYNA calculates the stresses and strains at every node in a model at many small time-intervals (time-steps) throughout the duration of the analysis. Livermore Software Technology Corporation (2002) explains the numerical method used to calculate time-step when an explicit analysis is performed.

LS-DYNA determines the force on each node from the previous time-step, which allows it to calculate the acceleration of the node (using force = mass x acceleration) and subsequently the displacement of that node (distance = speed x time). This displacement is converted to the strain of the element(s) the node belongs to. The stress in the element is calculated from the strain, which allows the force on the neighbouring node, in the next time-step to be determined. This process can be thought of like a wave propagating through the model.

However, the position of every node needs to be calculated at the same time, unaffected by calculations from the previous time-step. The time-step must therefore be set to allow calculations of adjacent nodes to be completed before the 'wave' from the previous calculation reaches them.

The 'wave' propagates through the material at the speed which sound travels through that material, which is dependent on its stiffness and density. This speed is given in Livermore

Software Technology Corporation (2006) for 3D-continuum elements as $c_{3D-continuum} = \sqrt{\frac{E(1-\upsilon)}{(1+\upsilon)(1-2\upsilon)\rho}}$ and for beam elements as $c_{beam} = \sqrt{\frac{E}{\rho}}$ where E = Young's modulus, υ = Poisson's ratio and ρ = density. The time-step is then calculated as $t = \frac{h}{c}$ where h is the element length.

If the mesh of the model is irregular, and so has elements of different sizes, LS-DYNA will use the shortest element to calculate the time-step. It will use this time-step for the entire model so it is preferable to create a uniform mesh to avoid an excessive amount of calculations being performed. Similarly, if there are different materials in the model, the material which gives the shortest time-step will be used to determine the time-step for the entire model.

To allow for possible errors in the time-step size calculation, the time-step can be multiplied by a factor given in the input file under the CONTROL_TIMESTEP keyword under TSSFAC (see Appendix 1). This is set to 0.9 as the default (0.8 has been used in analyses for this report).

3.4 Displacement Control

In the analyses for this report, rather than applying stress and measuring subsequent displacement, elements are analysed by being subjected to a prescribed displacement and measuring the resulting stress. This allows the (decreasing) stresses that arise beyond the displacement at which the ultimate strength is reached to be registered, otherwise the solution would diverge after this point.

4 ANALYSES

4.1 Single Element Tests

In order to gain an understanding of results of LS-DYNA analyses, and investigate the effects of changing element size, three single cube elements of different sizes were analysed in tension and compression.

4.1.1 Geometry and Boundary Conditions

The small cube was 50 mm, medium was 100 mm and large was 200 mm (Figure 4.1).

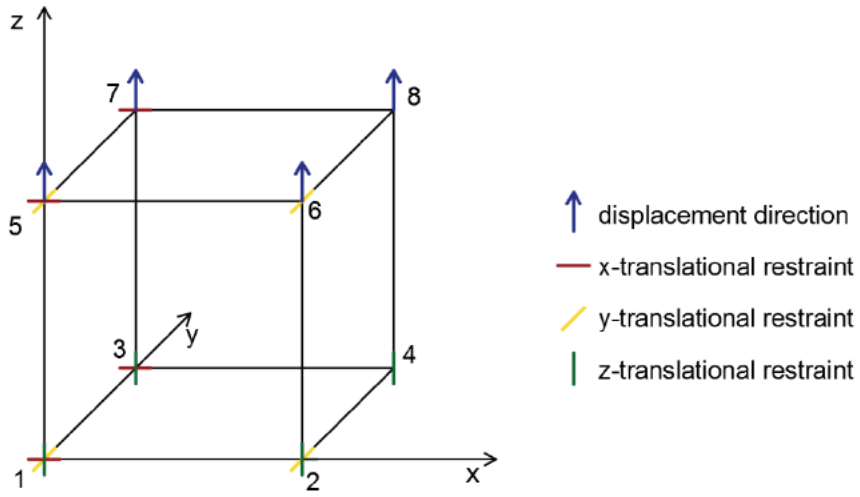

Figure 4.1 Single Cube Element.

A prescribed displacement was applied in the z-direction on the top face i.e. at nodes 5, 6, 7 and 8. This displacement was 0.5 mm for tension and -5.0 mm for compression, and was applied over 10 seconds.

Translational restraints were applied in the x-direction to nodes 1, 3, 5 and 7; in the y-direction to nodes 1, 2, 5 and 6; and in the z-direction to nodes 1, 2, 3, and 4. No rotational restraints were applied.

4.1.2 Input Parameters

The Concrete Damage Plasticity Model (CDPM2) was used with, initially, the properties given in Table 4.1.

Table 4.1 Input Parameters for Single Element

Concrete						
ρ_c kg/m^3	E_c GPa	υ_c	f_t MPa	f_c MPa	H_p	w_f m
2300	20	0.2	2.4	24	0.01	185.1×10^{-6}

The strengths were then increased for further analyses to 4.5 MPa and 30 MPa for tension and compression, respectively. The bi-linear damage formulation was used and the w_f value corresponds to a fracture energy of 100 Nm/m^2, calculated from (3.3).

All other input for the material was left as default. See Appendix 1 for the input files used in the single element analyses.

4.1.3 Results and Discussion

4.1.3.1 Tension

The stress-strain graphs of the cubes subjected to axial tension are plotted in Figure 4.2, showing the tensile stress in the z-direction against the axial strain in the z-direction.

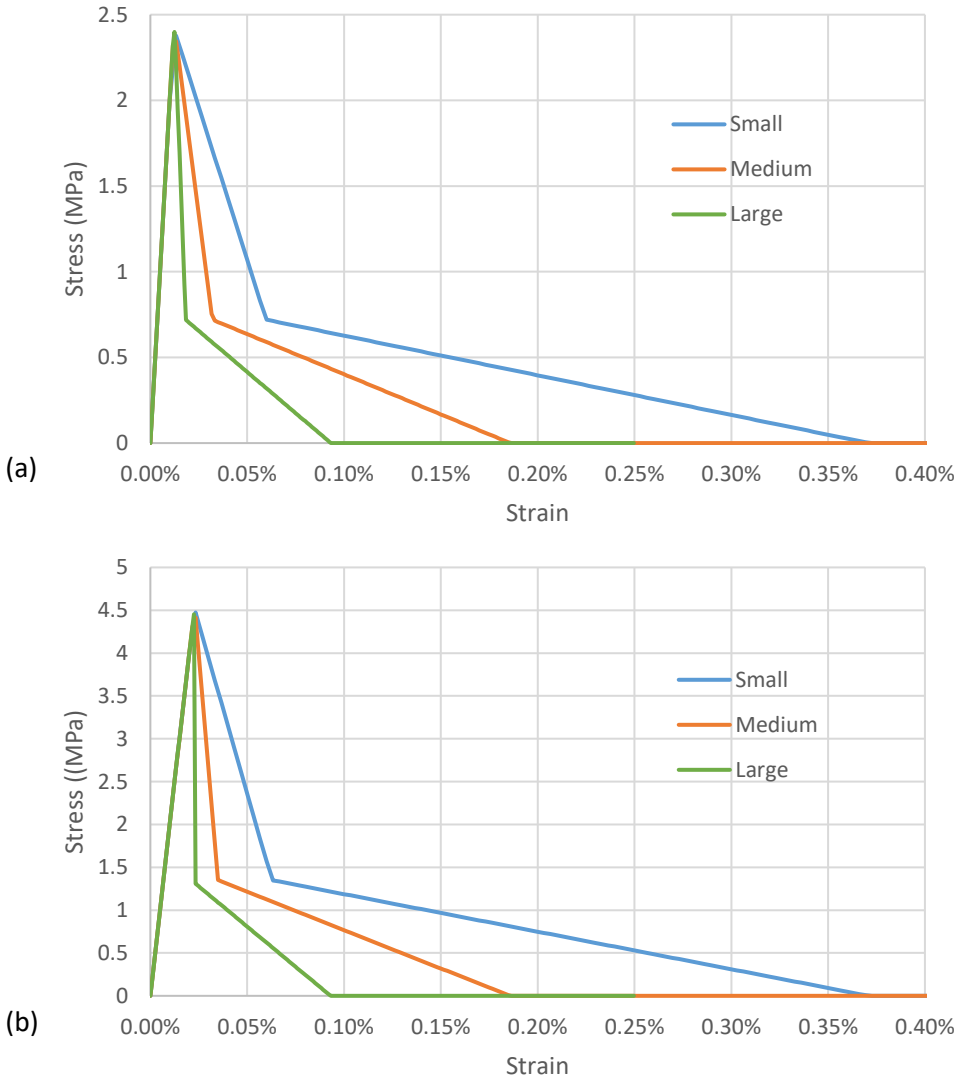

Figure 4.2 Stress-strain graph of cubes subjected to tension with tensile strength (a) 2.4 MPa (b) 4.5 MPa.

The time-steps during the analyses are very small, meaning there would be a very large number of points to plot if the data from all of them were used. Instead, only the data for some of the points are given in the output file from LS-DYNA i.e. the plotted time-step is effectively

much larger than the actual time-step used in the analysis. Markers for the plotted points are not shown: instead a line through each point is displayed to give a better indication of the results.

In all cases, the graph peaks at roughly the tensile strength of the cube, as expected. The shape of the graph after the peak is due to the bilinear stress-crack width response which was given as input to the analyses. The reduction of stress with increasing axial strain indicates strain softening. The displacement of the element is made up of the elastic displacement of the concrete plus the width of any cracks developed in it, as explained in section 2.2.1. Figure 4.3 shows the axial tensile stress in the z-direction against the crack width w_c for each element, which was produced by subtracting the elastic displacement from the total displacement for each response.

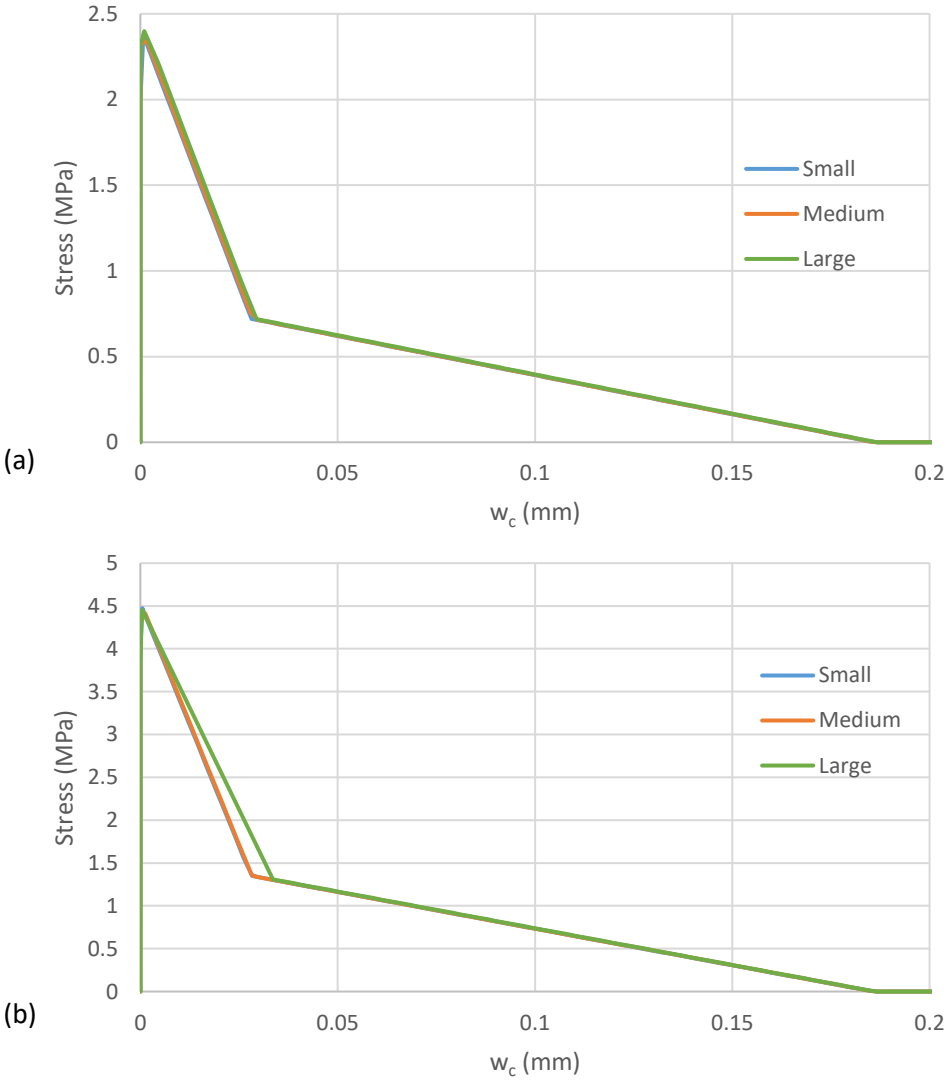

Figure 4.3 Stress vs. crack width of cubes subjected to tension with tensile strength (a) 2.4 MPa (b) 4.5 MPa.

The values of the stress-crack width graphs are concurrent with those given as input. As a reminder, these were: w_f = 185.1x10^{-6} m, w_{f1} = 0.15 x w_f = 2.78x10^{-5} m and f_{t1} = 0.3 x f_t = 7.2x10^5 MPa for the 2.4 MPa strength; and 1.35x10^6 MPa for the 4.5 MPa strength.

It can be seen in Figure 4.2 that the strain at which the stress becomes zero is different for each size of cube: doubling as cube size halves, but is unaffected by increase in tensile strength. All three cubes have the same w_f =185.1x10^{-6} m but since crack width expressed as a strain $\varepsilon_{wc} = \frac{w_c}{h}$ where w_c is the crack width and h is the original cube size, the strain decreases as original cube size increases. If stress is plotted against displacement (Figure 4.4) rather than strain, it can be seen that the displacement at which the stress becomes zero is the same.

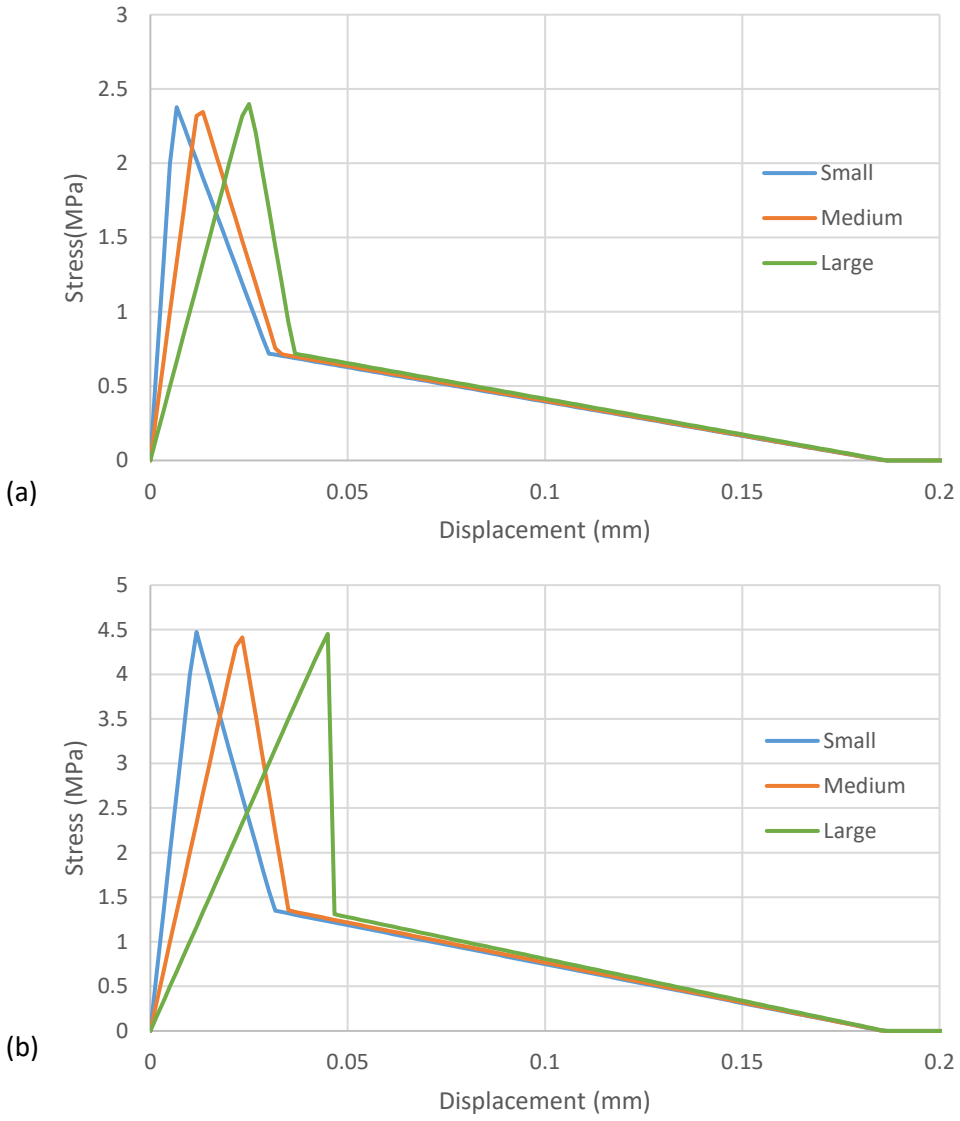

Figure 4.4 Stress-displacement graphs of cubes subjected to tension with tensile strength (a) 2.4 MPa (b) 4.5 MPa.

The maximum tensile stress is reached at different displacements for each cube: increasing as cube size increases, with the difference more significant with the higher tensile strength. This is because the total displacement Δl includes elastic displacement δ_e as well as the crack width, i.e. $\Delta l = \delta_e + w_c$, and the elastic displacement depends on the cube size i.e. $\delta_e = h\varepsilon_{wc}$. This is also the reason for the displacement at the start of the second branch of the strain softening part being larger than w_{f1}=2.78x10^{-5} m for all cubes. The stress in each cube becomes zero at the same displacement because the elastic part of the displacement is zero by this point, so total displacement is dependent only on crack width.

4.1.3.2 Compression

The stress-strain graphs of the cubes subjected to axial compression are plotted in Figure 4.5, showing the axial compressive stress in the z-direction against the strain in the z-direction.

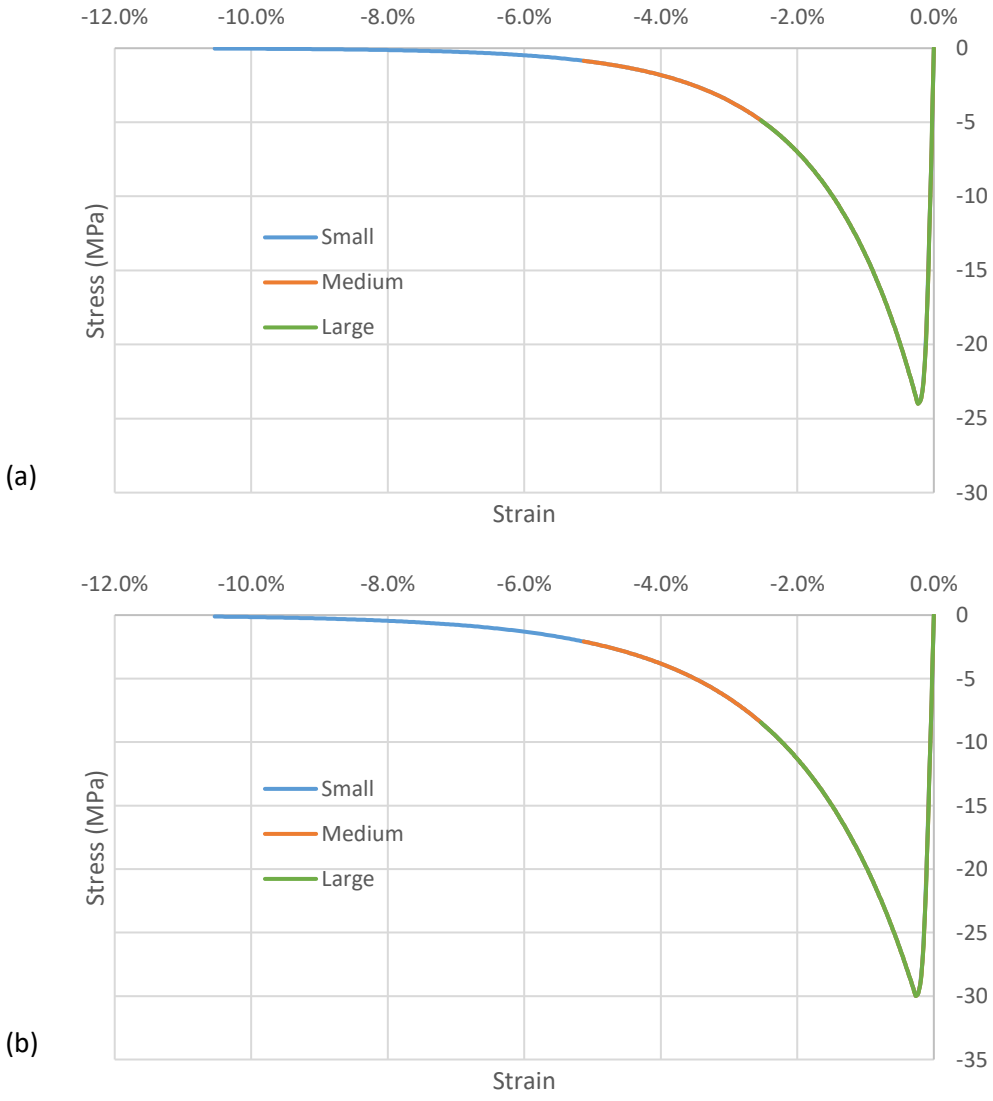

Figure 4.5 Stress-strain graph of cubes subjected to compression with compressive strength (a) 24 MPa (b) 30 MPa.

As expected, the peak stress is roughly the compressive strength. The shape of the graphs reflects the exponential compressive damage formulation given as input in the analyses. The response is unaffected by cube size. This is because the damage formulation was dependent on crack width expressed as a strain. However, just as for tension, when stress is plotted against displacement (Figure 4.6), the displacement at the compressive strength increases with increasing cube size. This is again because the total displacement includes elastic displacement, which depends on original cube size.

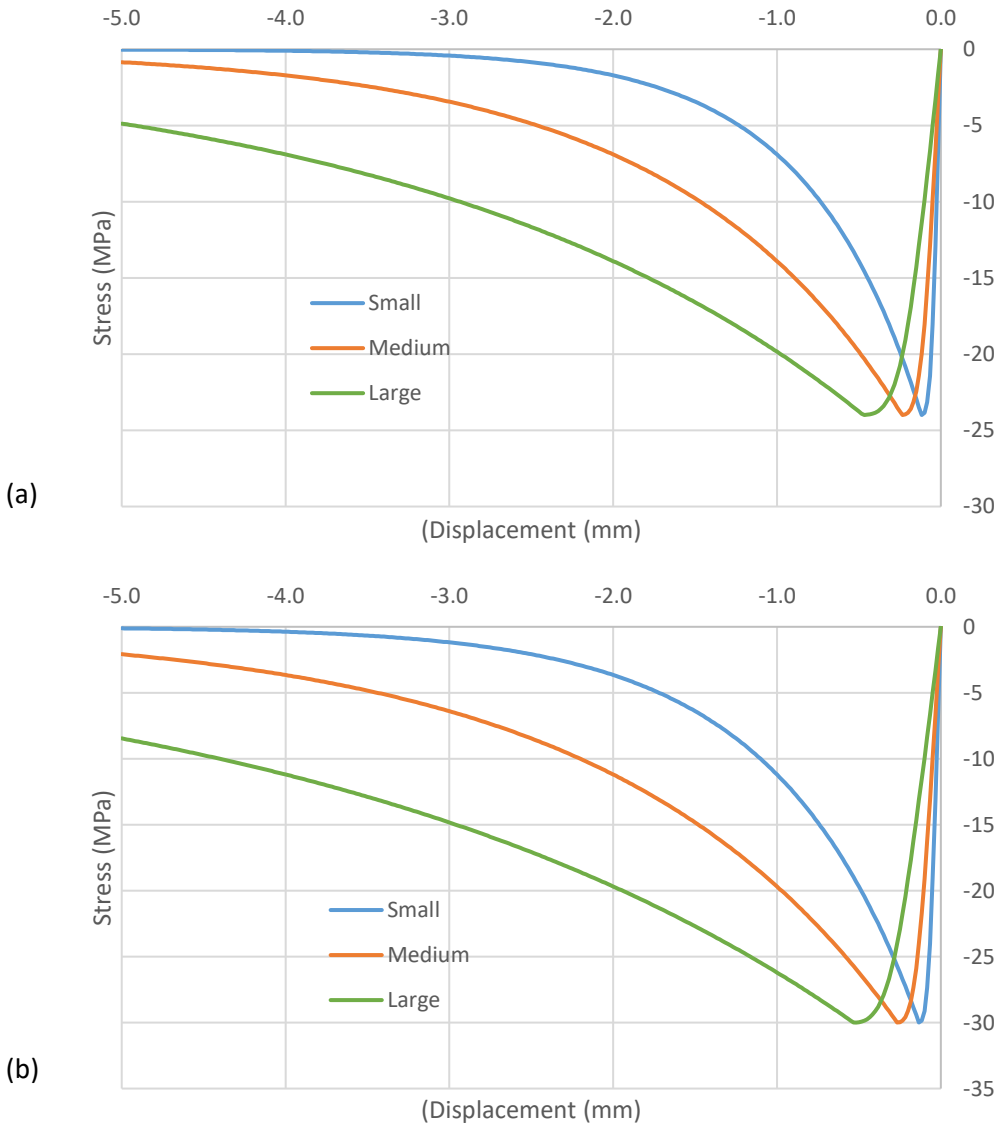

Figure 4.6 Stress-displacement graph of cubes subjected to compression with compressive strength (a) 24 MPa (b) 30 MPa.

4.1.3.3 Discussion

The displacements that result from either tension or compression in the different sized cubes are made up of the elastic displacement and the width of any cracks which develop.

In tension, the analysis uses a bilinear relationship between stress and crack width. This is why, when stress is plotted against strain, each cube size has the same strain at the tensile strength of the concrete but different strains at zero stress; and when stress is plotted against displacement, the displacement in each cube is different at tensile strength but the same at zero stress.

In compression, a damage relationship between stress and crack strain results in strains being the same for each cube size when stress is plotted against strain, but when stress is plotted against displacement, each size gives different displacements at compressive strength and the stress tends towards zero at decreasing strain with decreasing cube size.

Each cube in these analyses can represent an element from meshes of different sizes. It can therefore be concluded that CDPM2 can produce completely mesh-independent stress-strain results for compression, but for tension only the elastic part of the response is mesh-independent. The damage part is mesh-independent if a stress-displacement graph is created. However, the elastic part would then be mesh-dependent. This implies that where displacements localise within zones which are dependent on element length, CDPM2 will provide mesh-independent results.

4.2 Small Prism Tests

To verify mesh independency and investigate the methods of modelling reinforcement, prisms subjected to tension were modelled with different mesh sizes, with and without reinforcement. The plain prism (no reinforcement) was also used to check if changing the strain-rate would alter results.

4.2.1 Geometry, Mesh and Boundary Conditions

The prisms were 200 mm tall with a square base of 100 mm and are shown in Figure 4.7.

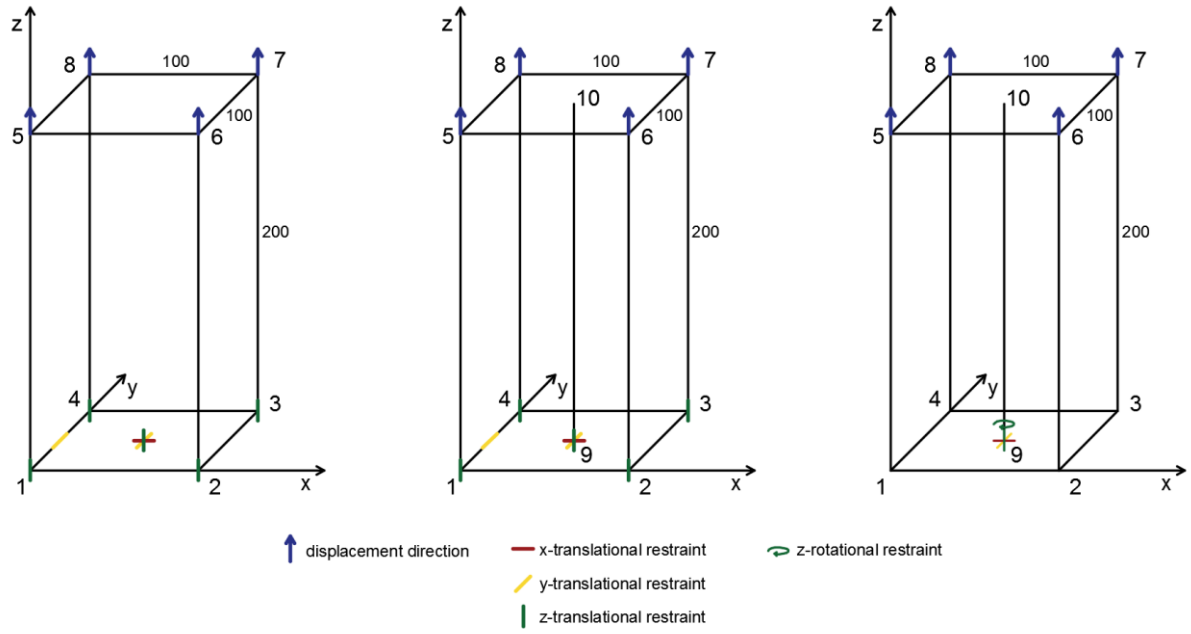

Figure 4.7 Small Prism (a) Plain (b) Reinforced with whole top face loaded (c) Reinforced with only the reinforcement loaded.

The mesh creation programme T3D was used to create uniform tetrahedral meshes for each case. The fine mesh was of size 0.01 m, the medium mesh was 0.02 m and the coarse mesh was 0.04 m. The meshes are shown in Figure 4.8.

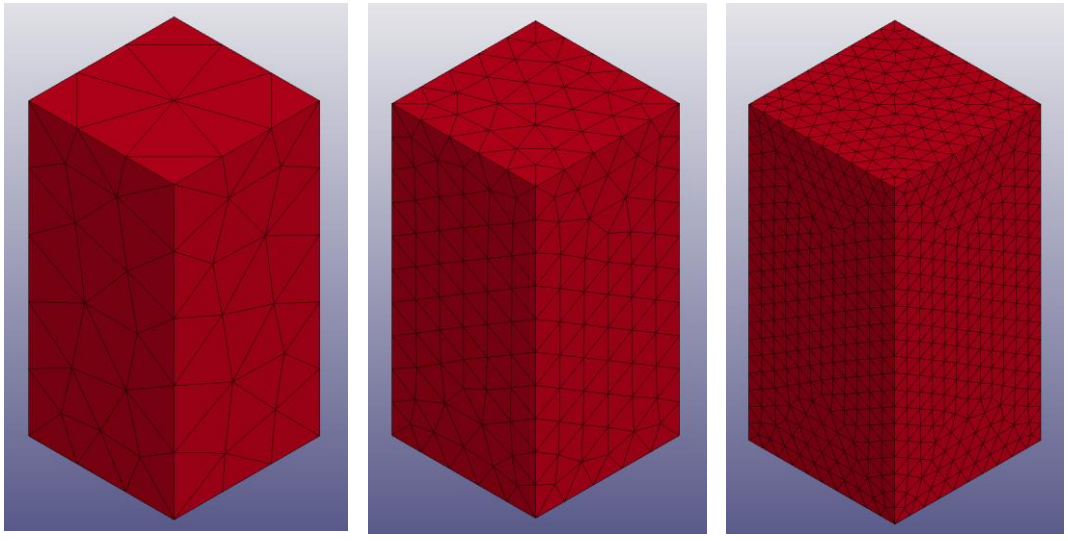

(a) (b) (c)

Figure 4.8 Meshes for small prism (a) coarse (b) medium (c) fine.

In the plain prism, the bottom face was restrained in the z-direction, the centre node on this bottom face was restrained in all translational directions and one node on a side parallel to the y-axis was restrained in the y-direction to prevent the prism from rotating about the centre of the bottom face. No rotational restraints were applied.

A displacement of 0.05 mm was applied over 1 second for the medium mesh, which is equivalent to applying a displacement of 0.5 mm over 10 seconds, but saves computational time as only the first tenth of the 10 second analysis needs to run. This was compared to applying a displacement of 0.5 mm over 1 second, for all meshes, to check if there was an effect of increasing the strain-rate to confirm that loading the concrete for a shorter time would not alter results. An even faster rate was applied by applying a displacement of 5 mm over 1 second, to check if it would still provide accurate results.

For the case with reinforcement, 20 mm diameter beam elements were placed in the centre of the prism (nodes 9 to 10 in Figure 4.7(b) and (c)).

A prescribed displacement of 0.5 mm was applied over 1 second in the z-direction. For the prism with perfect bond using shared nodes, this was applied to the whole top face, with the same restraints as for the plain prism. It was then applied to the end of the reinforcement only, to check if this had any effect. For the perfect bond case with constrained nodes and the case with bond-slip, the displacement was applied to the reinforcement only. When only the reinforcement was loaded, restraint was applied only to the middle node on the bottom. It was restrained translationally in all directions and rotationally about the z-axis.

4.2.2 Input Parameters

The CDPM2 material model was used for the concrete and the MAT_PLASTIC_KINEMATIC material was used for the reinforcement, with the properties given in Table 4.2. See Appendix 2 for the input files.

Table 4.2 Input Parameters for Small Prism

Concrete							Reinforcement				Bond	
ρ_c kg/m^3	E_c GPa	υ_c	f_t MPa	f_c MPa	H_p	w_f m	ρ_s kg/m^3	E_s GPa	υ_s	f_y MPa	τ_{max} MPa	s_1
2300	20	0.2	2.4	24	0.01	103.7x10^{-6}	7850	200	0.3	500	8	0.6

The bi-linear damage formulation was used for the concrete and the w_f value corresponds to a fracture energy of 100 Nm/m^2, calculated from (3.3), having been scaled by 0.56 as

recommended for tetrahedral elements. All other material input for the concrete was left as default.

Rate effects were not considered for the reinforcement, eroding elements were not used and all other input for the reinforcement was set to default.

For the case with bond-slip, the relationship used (described in section 3.1.3) gives the maximum bond stress as $\tau_{max} = 2\sqrt{(f_c - 8)}$ which for concrete of this strength (24 MPa) is 8 MPa.

4.2.3 Results and Discussion

4.2.3.1 Plain

The force-displacement graphs for the plain prisms of medium mesh loaded at different rates are plotted in Figure 4.9.

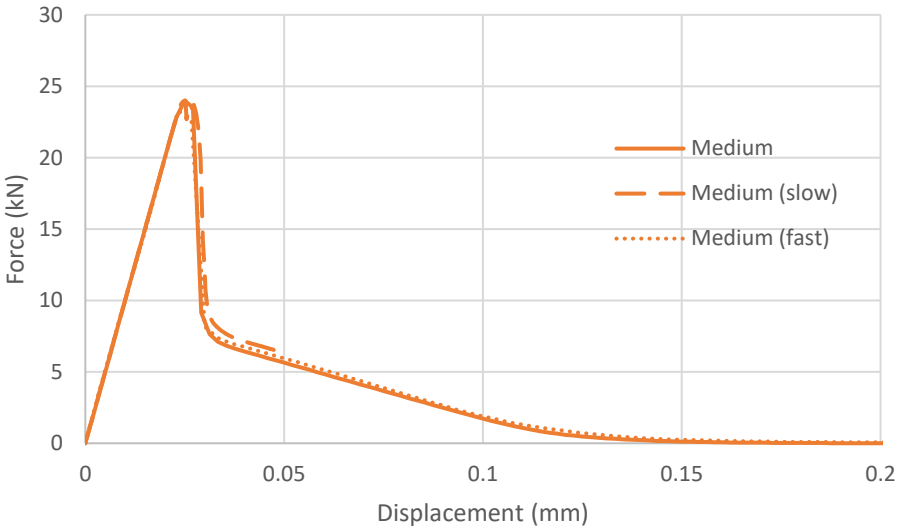

Figure 4.9 Force-displacement graphs for the small prism of medium mesh loaded at different rates

The fast analysis required to be plotted more frequently over the total displacement than the intermediate and slow analyses so that enough data points would be plotted at the start, before force became zero. The graphs for the intermediate and fast speeds agree well with the slower speed. This demonstrates that the intermediate strain-rate does not affect results significantly so it was deemed acceptable to use the intermediate speed for all analyses to save computational effort but still provide sufficient accuracy.

Figure 4.10 shows the force-displacement graphs for the prism loaded at the intermediate rate using coarse, medium and fine meshes.

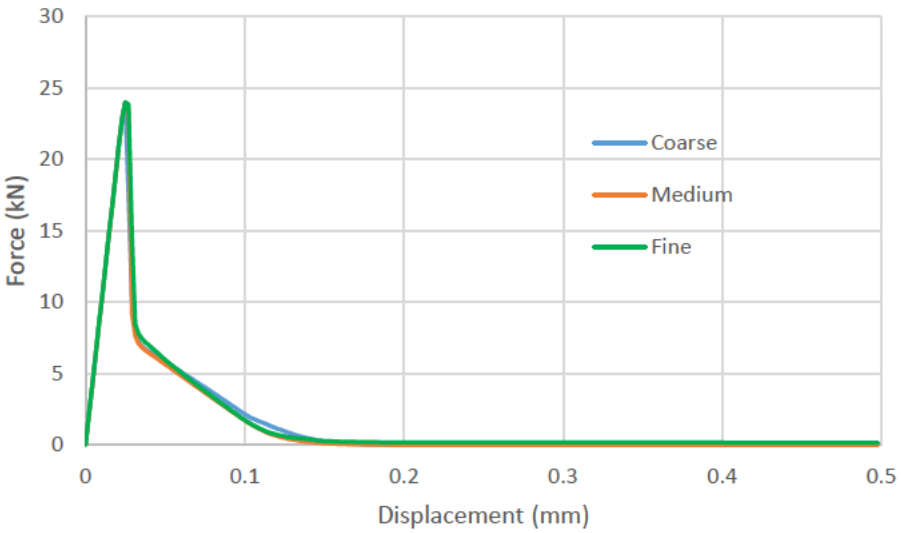

Figure 4.10 Force-displacement graphs for the small prism using different mesh sizes

It is clear that the response is mesh-independent since the coarse, medium and fine meshes produce very similar graphs.

Figure 4.11 shows the final stage of each contour plot of maximum principle strain for each mesh. The elements in red have maximum principle strains which represent cracks greater than or equal to 0.3 mm. Deformation is scaled to ten times bigger than actual size.

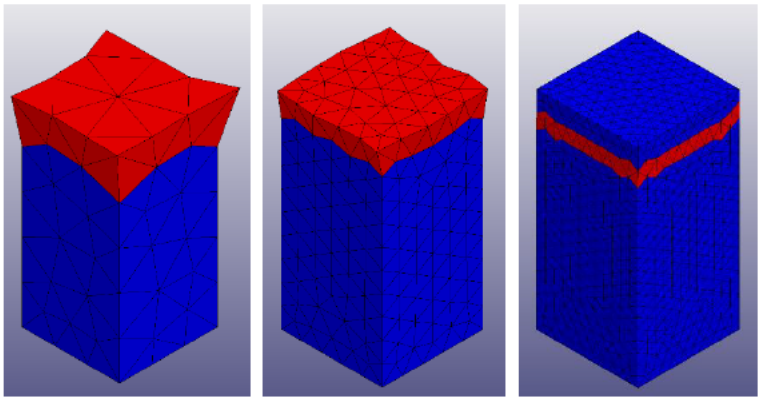

Figure 4.11 Contour plots of maximum principle strain of plain prisms subjected to tension with (a) coarse (b) medium (c) fine mesh.

It should be noted that the relatively large lateral deformations in the coarse and medium meshes are due to the deformation occurring in the elements at the end of the prism, which can occur in explicit codes such as LS-DYNA for nodes in which the displacements are prescribed. This could be avoided by using erosion (deleting elements with zero stiffness because both damage parameters become equal to 1); by increasing the stiffness in the

elements at the ends or reducing the stiffness of the middle elements; or by changing the ends to an elastic material. However, the purpose here is to show that all the meshes show one crack occurring, therefore demonstrating mesh-independence.

4.2.3.2 Reinforced

The force-displacement graphs for the prisms modelled with perfect bond using shared nodes are plotted in Figure 4.12. The two loading approaches are shown for the medium mesh. The expected response of a 20 mm diameter reinforcement bar without any concrete surrounding it (bare steel) is also plotted. The force at which yielding occurs was calculated as: $F_y = f_y A = 500 \times \pi \times 10^2 = 157$ kN. The displacement at which yielding occurs was calculated as: $\delta_y = \frac{F_y L}{E_s A} = \frac{500 \times \pi \times 10^2 \times 200}{200000 \times 500 \times \pi \times 10^2} = 0.5$ mm.

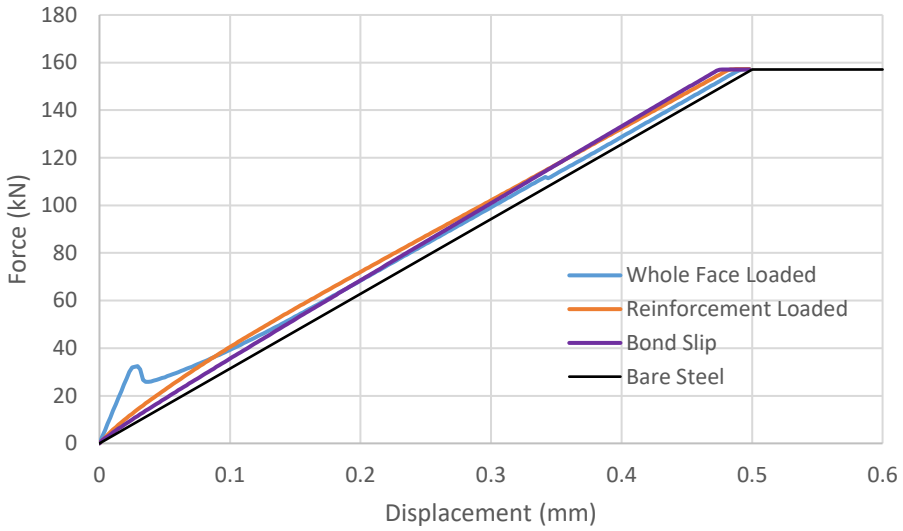

Figure 4.12 Force-displacement graphs for prisms modelled with perfect bond using shared nodes.

The loading methods produce similar responses to each other, with yield force and displacement of around the same as for bare steel, as expected. The slight difference in displacement is due to the fact that shrinkage has not been considered, as discussed in section 2.2.5. The responses are very similar to each other apart from the very start where the response of the prism with displacement applied to the whole top face is steeper. The kink represents a crack in the concrete. However, Figure 4.13 shows the final stage of the contour plot of maximum principle strain of each loading method, using the medium mesh, in which there are two cracks (of width 0.2 mm or greater, represented by red colour) for the prism with the whole top face loaded, instead of just one. The prism with only the reinforcement loaded shows no cracks which corresponds to the force-displacement graph so it was decided that this loading method is most suitable.

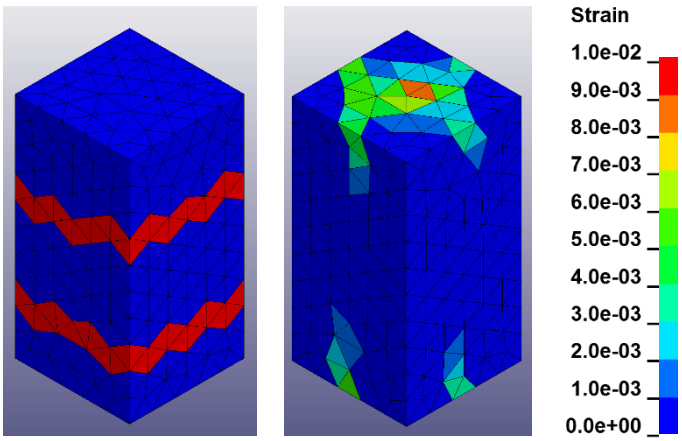

Figure 4.13 Contour plots of maximum principle strain for prisms modelled with perfect bond using shared nodes with tension applied to (a) the whole top face (b) the ends of the reinforcement only.

The force-displacement graph for each method of modelling the reinforced concrete, (with only the reinforcement loaded) is shown in Figure 4.14. The results shown are for the medium mesh.

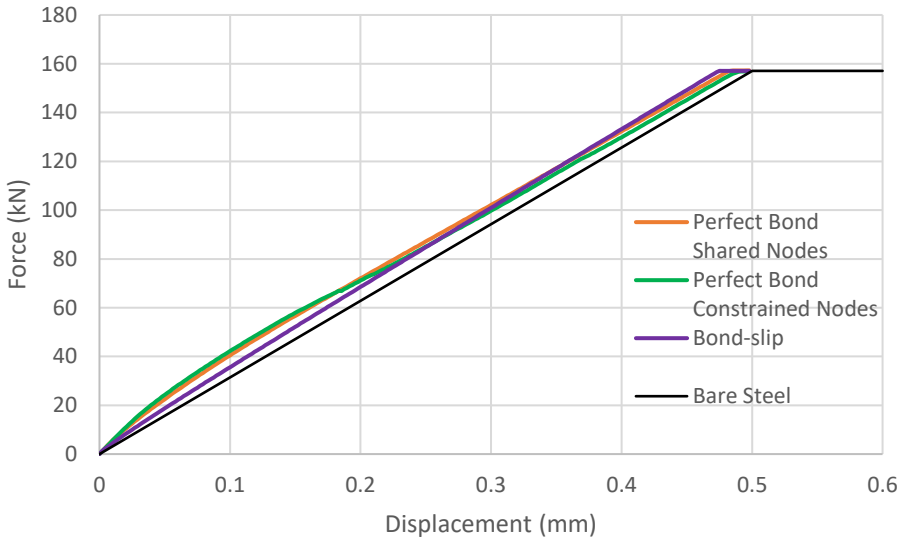

Figure 4.14 Force-displacement graphs for each method of modelling reinforced concrete.

There is good agreement between the two perfect bond approaches, suggesting that the constrained nodes method can be deemed an acceptable method for modelling perfect bond. The response with bond-slip is similar to the perfect bond responses, suggesting that it is also an acceptable method.

The contour plot of maximum principle strain for each modelling approach, using the medium mesh, are shown in Figure 4.15 where red elements contain displacement of 0.03 mm or greater.

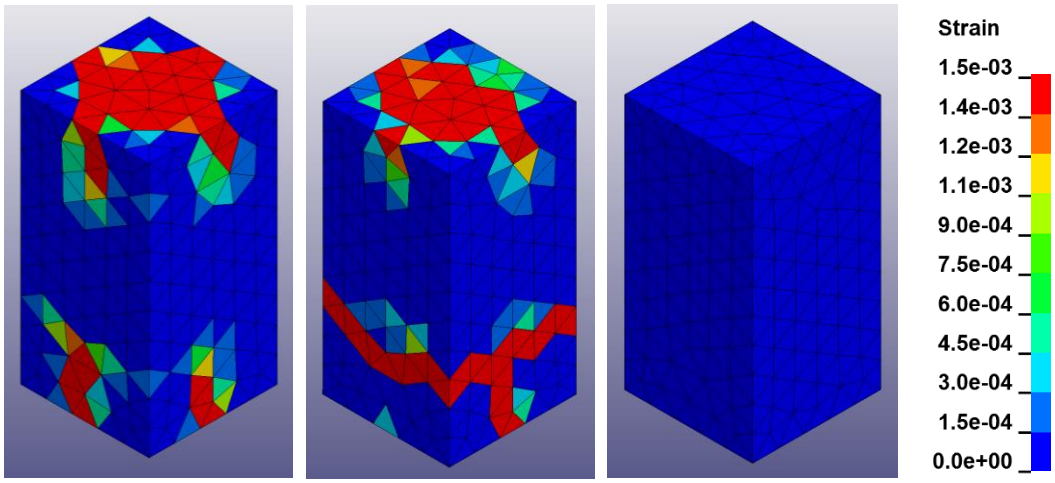

Figure 4.15 Contour plots of maximum principle strain for prisms with (a) perfect bond using shared nodes (b) perfect bond using constrained nodes (c) bond-slip using constrained nodes.

The prism with bond-slip shows no displacement because the strains in it are much smaller than in the other two prisms. Figure 4.16 shows the contour plot of maximum principle strain for the prism with bond-slip where red elements indicate displacement of 0.0012 mm or greater, showing that the formation of cracks of a much smaller width than the perfect bond prisms does not even occur.

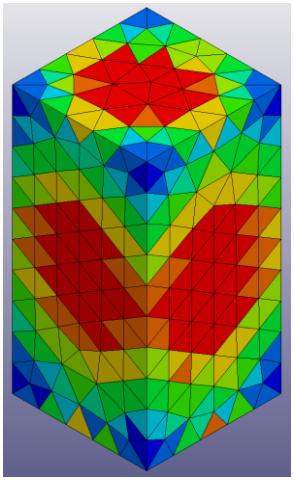

Figure 4.16 Contour plot of maxmum principle strain for prism with bond-slip.

The models with perfect bond show displacement at the ends of the prism. This is expected since the perfect bond restricts the relative displacement of the concrete and reinforcement to zero. Since the reinforcement undergoes displacement, the concrete must displace equally. The lack of end displacement (of at least 0.03 mm) in the approach with bond-slip is

appropriate since the concrete is allowed to displace relative to the reinforcement. The perfect bond approach with shared nodes and the approach with bond-slip both show no cracks i.e. no cracks in the plane perpendicular to loading (the shared nodes prism only shows cracks in the longitudinal direction which are due to the end displacement). This is concurrent with the force-displacement graphs which have no kinks. The perfect bond approach with constrained nodes shows one lateral crack. This is not concurrent with the force-displacement graph which has no kinks. However, it may not always be the case that force-displacement graphs show cracks as kinks.

The force-displacement graphs for the coarse, medium and fine meshes for each modelling approach are shown in Figures 4.17, 4.18 and 4.19.

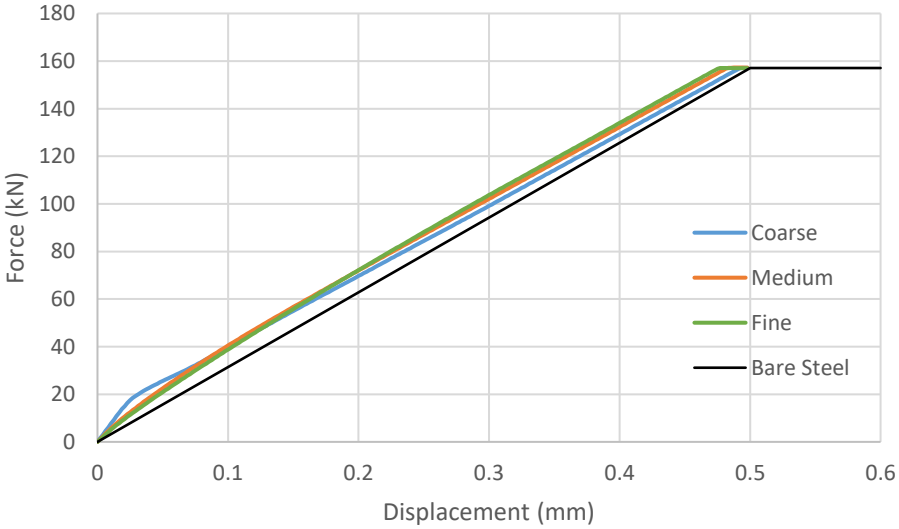

Figure 4.18 Force-displacement graphs for perfect bond with shared nodes.

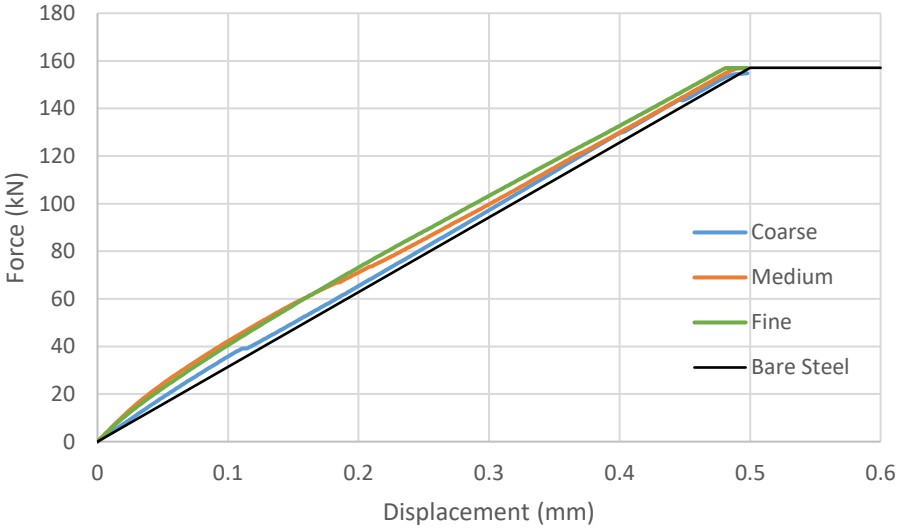

Figure 4.17 Force-displacement graphs for perfect bond with constrained nodes.

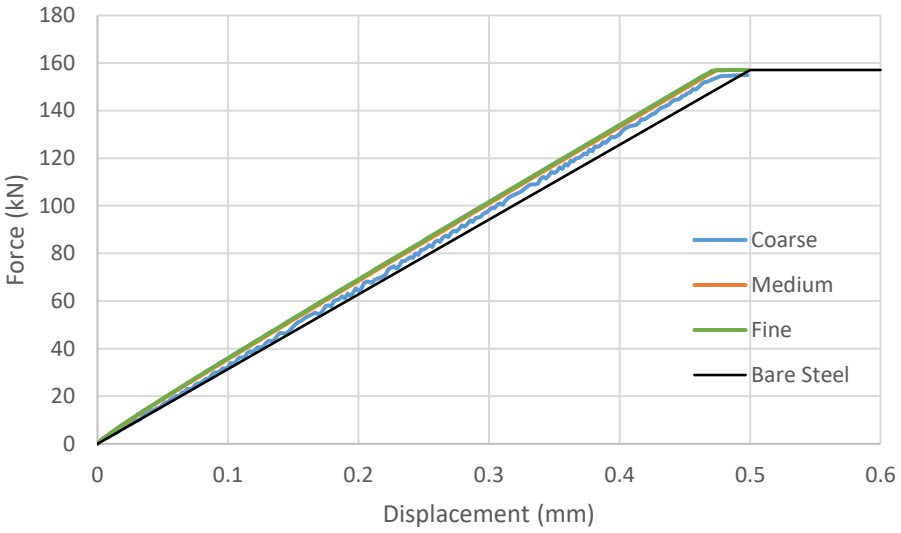

Figure 4.19 Force-displacement graphs for prisms with bond-slip.

All modelling approaches produced mesh-independent results as the responses from each mesh size agree well with each other, especially in the approach with bond-slip.

4.2.3.3 Discussion

It was decided that the intermediate loading rate did not affect results significantly so it was used to save computational effort. The subsequent force-displacement graphs for the plain prism demonstrated mesh-independency.

Loading only the ends of the reinforcement in the reinforced concrete analyses was chosen as the best method as it produced the expected force-displacement graph. Modelling the reinforced concrete with bond-slip using constrained nodes was deemed suitable. These methods were used and the resulting force-displacement graphs for coarse, medium and fine meshes demonstrate mesh independency.

4.3 Tension Stiffening Tests

In order to validate CDPM2 for modelling reinforced concrete subjected to tension, a physical experiment was modelled and the results of the analysis compared to the physical experiment. The experiment chosen subjected concentrically reinforced concrete prisms to tension and investigated tension stiffening and cracking of the concrete and is reported in Bischoff (2003).

4.3.1 Geometry, Mesh and Boundary Conditions

In Bischoff's experiment, the prisms had a square cross-section of side 100 mm and were 1100 mm long, as shown in Figure 4.20. The reinforcement bars were 16 mm in diameter (Canadian size 15M). Reinforcement bars of 19.5 mm diameter (20M) were also tested but are not used for comparison in this report. The bars were 1020 mm long and attached to bars of larger diameter (19.5 mm) which protruded from each end to allow the axial tensile force P to be applied there. These thicker bars were used at each end to ensure that the main reinforcing bar would not yield before the intended load could be applied.

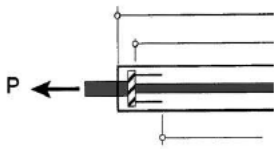

Figure 4.20 Tension Stiffening Experiment Specimen (Bischoff, 2003).

Bischoff (2003) measured average member strain over the middle 900 mm of the prism, recorded continuously at 0.5 s intervals throughout loading. The number of observed cracks, crack widths and crack spacings were also recorded.

The experiment used both plain concrete and steel fibre-reinforced concrete. Comparisons are made with both of these in this report but mostly focus on the response of the plain concrete.

The mesh creation programme T3D was again used to create a tetrahedral mesh. A uniform mesh of size 0.02 m was used, shown in Figure 4.21.

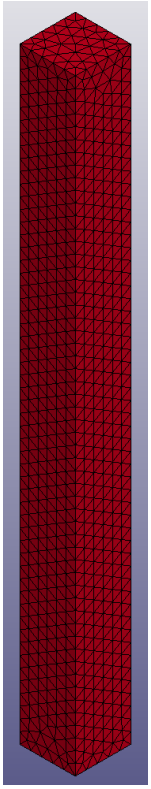

Figure 4.21 Mesh for tension stiffening test model.

For the reinforcement, beam elements were placed in the centre of the prism. These were given a diameter of 16 mm and to account for the thicker bars at the ends of the specimen in the experiment, the cross-section was increased to 20 mm in diameter in two elements at each end.

A prescribed displacement which would cause the reinforcement to yield was required to ensure the full response of the prisms could be observed. The displacement at which the reinforcement would yield was calculated from $d_y = \frac{f_y L}{EA}$ where A is the area of reinforcement equal to 200 mm^2, E is the Young's Modulus, F_y is the force at which yielding occurs $\left(F_y = f_y A = 84.5kN\right)$ and L is the length of the prism, 1100 mm. This gives a displacement of 2.29 mm so 2.5 mm was used in the analyses to ensure yielding would be observed. This was applied over 1 second for all analyses.

4.3.2 Input Parameters

The CDPM2 material model was used for the concrete and the MAT_PLASTIC_KINEMATIC material was used for the reinforcement with the properties given in Table 4.3, for the plain concrete (no fibre-reinforcement). See Appendix 3 for the input files.

Table 4.3 Input Parameters for Plain Concrete Tension Stiffening Model

Plain Concrete							
ρ_c kg/m^3	E_c GPa	υ_c	f_t MPa	f_c MPa	H_p	w_f m	ε_{fc}
2300	39.7	0.2	5.42	62.8	0.01	70.1x10^{-6}	0.01
Reinforcement						**Bond**	
ρ_s kg/m^3	E_s GPa	υ_s	f_y MPa			τ_{max} MPa	s_1
7850	200	0.3	500			14.8	0.6

A fracture energy of 153.8 Nm/m^2 and a Young's modulus of 39.7 GPa were obtained from (3.1) and (3.4), and the compressive strength of 62.8 MPa. Since the tensile strength is 5.42 MPa and fracture energy as given above, the w_f value was obtained from (3.3) and scaling by 0.56. ε_{fc} was given a higher value of 0.01 instead of the default to make the initial gradient of the stress-crack strain curve less steep and allow the analysis to run more quickly. Rate effects were not considered for the reinforcement, eroding elements were not used and all other material input was set to default.

Table 4.4 gives the input parameters for the fibre-reinforced concrete test. The compressive strength gave a fracture energy of 153.6 Nm/m^2 and Young's modulus of 39.6 GPa from (3.1) and (3.4). To account for the fibre reinforcement, the second branch of the bi-linear damage formulation was 'flattened' by giving w_f a very high value of 1x10^6 m. The value of w_{f1} could therefore not be the default 0.15w_f. From the fracture energy and tensile strength, a w_f value of 70.1x10^{-6} m would be used if the concrete was plain, so w_{f1} was 15% of this which is 6.48x10^{-6} m.

Table 4.4 Input Parameters for Fibre-reinforced Concrete Tension Stiffening Model

Fibre-reinforced Concrete								
ρ_c kg/m^3	E_c GPa	υ_c	f_t MPa	f_c MPa	H_p	w_f m	W_{f1} m	ε_{fc}
2300	39.6	0.2	8.85	62.4	0.01	1x10^6	6.48x10^{-6}	0.01
Reinforcement							**Bond**	
ρ_s kg/m^3	E_s GPa	υ_s	f_y MPa				τ_{max} MPa	s_1
7850	200	0.3	500				14.8	0.6

The prisms were modelled with perfect bond using both the shared node and constrained node approaches. They were also modelled with bond-slip, with the bond-slip relationship altered in various ways to investigate the effect of this. The fibre-reinforced concrete was modelled with bond-slip. Only the reinforcement was loaded for all analyses and restraints were the same as for the small prism in section 4.2.

The same simplified bond-slip relationship as the small prism was used for the plain and fibre-reinforced concrete. Initially the recommended values were used: s_1=0.6 mm, $\tau_{max} = 2\sqrt{(f_c - 8)} = 14.8$ MPa. The maximum bond stress was then increased to 29.6 MPa and decreased to 7.4 MPa with s_1 kept at 0.6 mm. With $\tau_{max} = 14.8$ MPa, s_1 was increased to 1.2 mm.

It is expected that the fibre-reinforced concrete will produce a higher yield stress than the plain concrete, due to the fact that inclusion of steel fibres in the concrete allows tension to be carried across cracks. It is also expected that the fibre-reinforced concrete will produce cracks of smaller width than the plain concrete as a result of reduced crack spacing and increased tension stiffening.

4.3.3 Results and Discussion

Figure 4.22 shows the force-displacement response from the perfect bond models with shared nodes and constrained nodes.

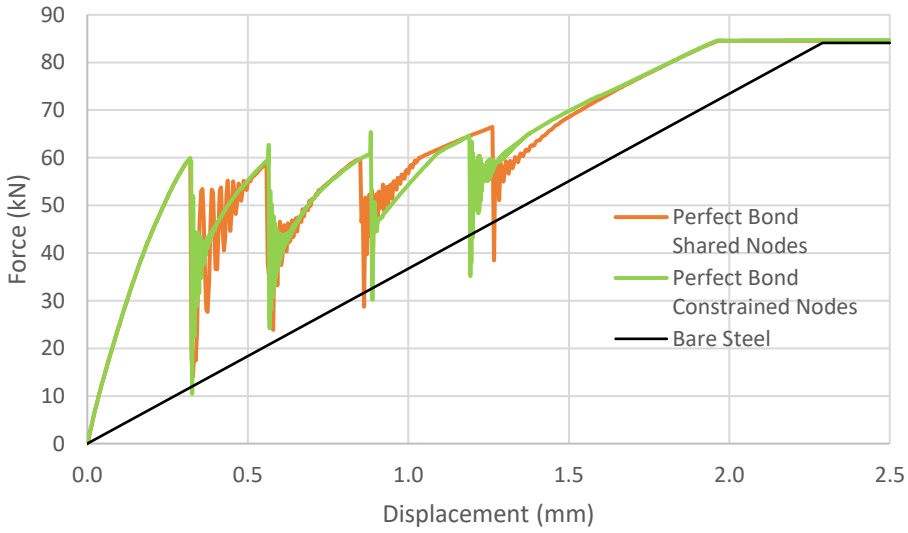

Figure 4.22 Force-displacement graphs for prisms modelled with perfect bond.

There is reasonable agreement between the two responses with initial cracking at the same force and displacement of around 60 kN and 0.3 mm respectively; the same number of kinks which represent cracks in the concrete; and yield at the same force and displacement of around 85 kN and 1.9 mm respectively. Therefore, it was decided that the constrained nodes method is acceptable. This method was used to include bond-slip and the resulting force-displacement graph is shown in Figure 4.23, along with the estimated bare steel response.

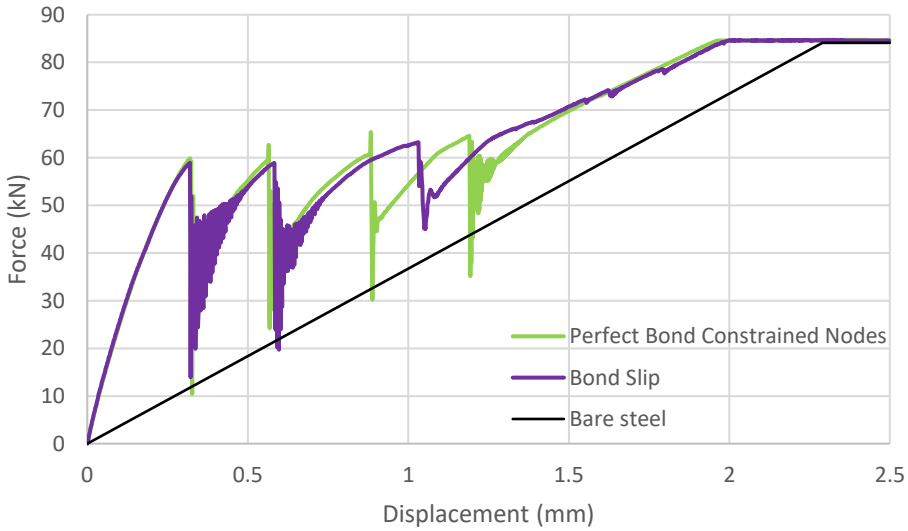

Figure 4.23 Force-displacement graphs of prisms modelled with constrained nodes.

The model with bond-slip gave a similar response to perfect bond but with one less crack. This is expected because the restriction of the relative displacement between reinforcing bar and concrete should cause more cracks to ensure that the overall member elongation is equal for both steel and concrete. The graphs are concurrent with the contour plots of maximum principle strain (Figure 4.24) where there are 4 major cracks for perfect bond at the stage when the reinforcement yields (around 0.78 s) and 3 for bond-slip. Cracks greater than or equal to 0.3 mm are indicated by red elements. Any cracks which form after yield e.g. in the elements coloured green, orange and yellow, are secondary cracks and are ignored.

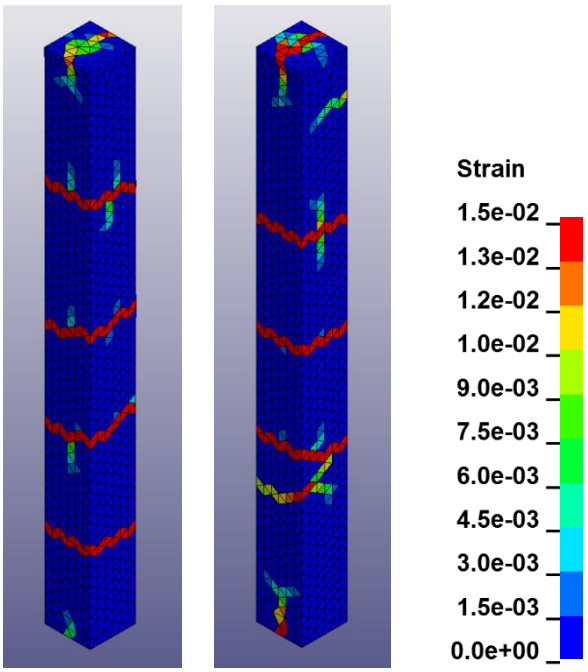

Figure 4.24 Contour plots of maximum principle strain for prisms modelled with (a) perfect bond (b) bond-slip.

The agreement between the perfect bond and bond-slip responses gave sufficient reason to assume that responses produced from the models which included bond-slip are suitable for comparison to the Bischoff experiment.

Figure 4.25 shows the responses of the plain and fibre-reinforced concrete (FRC) models along with the results from Bischoff's experiment, and the bare steel response. In Bischoff's experiment, the results were adapted to consider shrinkage effects (see section 2.2.5). However, these have not been considered in the analyses so results should be adapted for a better representation of the responses. This is the reason for the mismatch at the beginning of the graph in Figure 4.25. Aside from this, the response of the plain concrete model agrees well with the plain concrete response in the experiment. Both plain concrete responses indicate the formation of cracks, the occurrence of tension stiffening and force at yield of around 85 kN. The strain at yield is also similar at around 1.8 mm and 1.9 mm for the model and experiment respectively. The plain concrete experiment resulted in six cracks within the 900 mm gauge length. The model agrees fairly well with this, with three cracks, as shown in Figure 4.24(b).

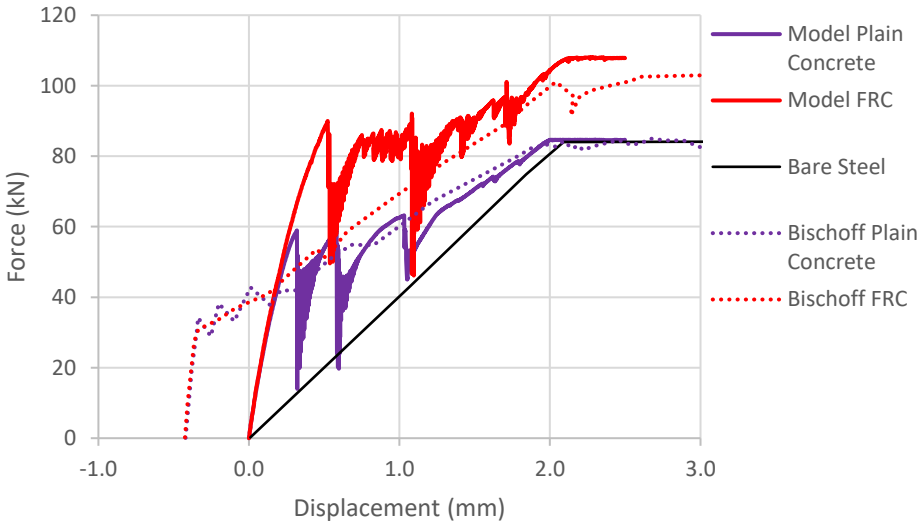

Figure 4.25 Axial load vs. member strain graphs from the Bischoff experiments and LS-Dyna analyses.

The response of the model with fibre-reinforcement agrees with the plain concrete response initially, as it does in the experiment. However, the force and displacement at first cracking are higher than for plain concrete, at around 90 kN and around 0.52 mm for the FRC compared to around 60 kN and 0.26 mm for the plain concrete, respectively. In the experiment, the two responses diverged much more slowly. However, other studies (Mitchell et al., 1996), which used a higher percentage of steel fibres than Bischoff used, produced higher cracking stresses than for plain concrete. The percentage of steel fibres was not specified in the analysis so this could be the reason for the disagreeing model and experiment results. The force at yield in the experiment was higher than for the plain concrete, but at roughly the same strain, which is captured by the model response. However, the model gives a force at yield even greater than that observed in the experiment. The fibre-reinforced concrete specimens in the experiment developed eleven cracks. This higher number of cracks, and therefore shorter

crack spacing, was displayed in the model. The contour plot of maximum principle strain in Figure 4.26 shows that a total of fourteen cracks have formed at the time of yielding.

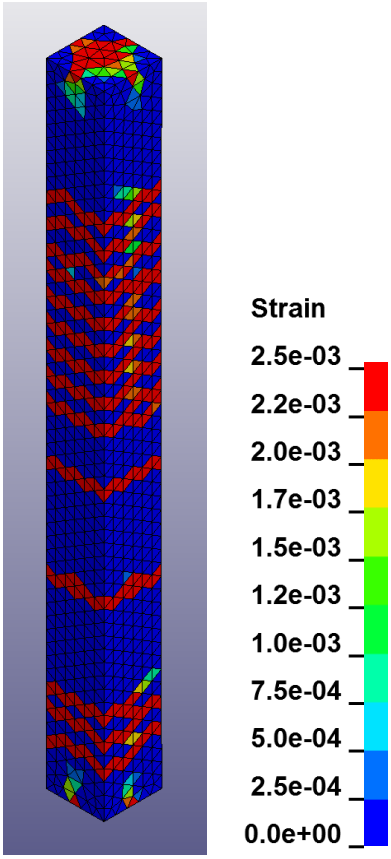

Figure 4.26 Contour plot of maximum principle strain for prism with fibre-reinforced concrete.

The fibre-reinforcement was expected to have smaller crack widths than plain concrete. This is also displayed by the model. In Figure 4.26, red coloured elements indicate cracks of greater than or equal to 0.05 mm, with the widest crack being around 0.3 mm. This is reduced in comparison to the plain concrete in which all cracks were at least 0.3 mm.

Figure 4.27 shows the force-displacement graphs for the plain concrete models with different bond-slip relationships.

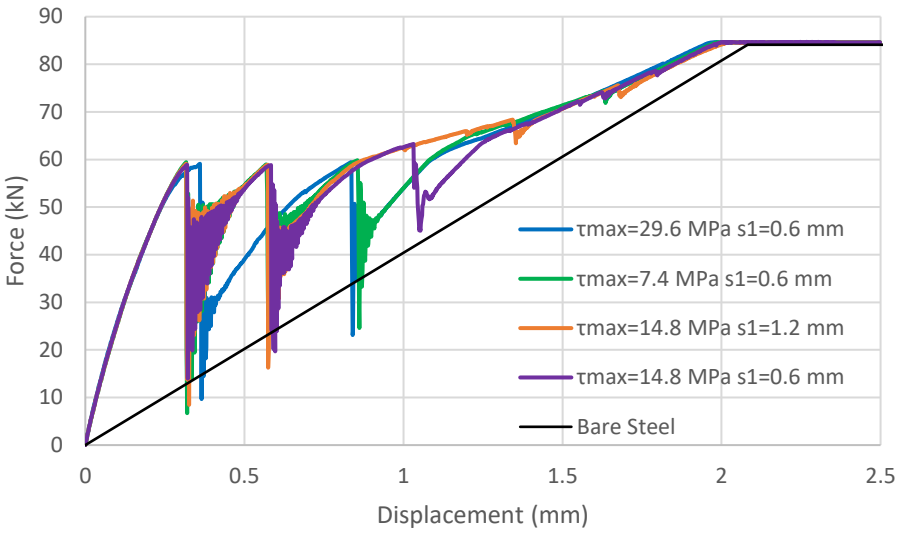

Figure 4.27 Force-displacement graphs for models with different bond-slip relationships.

All results show the same force at yield as for the bare steel response. This is expected since tension stiffening in plain concrete cannot continue after yielding of the reinforcement because forces can neither be transferred across cracks in the concrete nor carried through the steel. However, Bischoff (2003) states that bond affects crack spacing - and therefore number of cracks. This was demonstrated by the model in which s_1 was changed but was not captured significantly by the models with changes in τ_{max}. This is clearly seen in Figure 4.28 where the contour plots of maximum principle strain show three major cracks for s_1=0.6 mm (a), (b) and (c) and two for s_1=1.2 mm (d) at the point of yield. Red represents elements containing cracks of width 0.3 mm or greater.

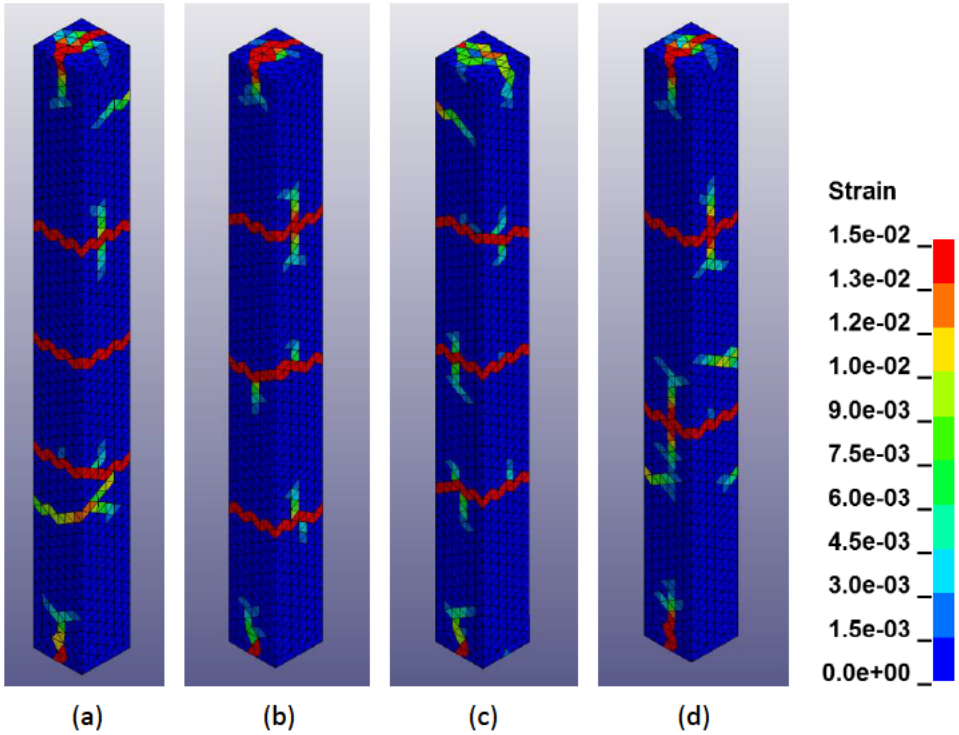

Figure 4.28 Contour plots for tension stiffening test models with (a) τ_{max}= 14.8 MPa, s_1 = 0.6 mm (b) τ_{max}= 7.4 MPa, s_1 = 0.6 mm (c) τ_{max}= 29.6 MPa, s_1 = 0.6 mm (d) τ_{max}= 14.8 MPa, s_1 = 1.2 mm.

4.3.3.1 Discussion

Modelling the reinforced concrete with bond-slip using constrained nodes was deemed suitable for comparison to Bischoff's experiment.

Despite the results not including shrinkage effects, the plain concrete model produced a similar number of cracks as the experiment, showed the occurrence of tension stiffening, and gave the same force at yielding of the prism. This suggests that CDPM2 is capable of producing results which agree with tension stiffening tests, although shrinkage effects should be considered to provide a proper validation.

The fibre-reinforced concrete model captured the increase in yield force, the higher number of cracks and smaller crack widths compared to the plain concrete. A higher cracking force and force at yield than reported in the experiment were observed. However, this could have been due to the percentage of steel fibres in the concrete being unspecified.

Changes in bond did not affect the force at yield, as expected. Crack spacing was altered by changes in bond, as expected, but only significantly by changes to the bond-slip variable, s_1.

5 CONCLUSIONS

5.1 General Conclusions

The aim of this project was to evaluate the suitability of CDPM2 for modelling the response of reinforced concrete structures to dynamic loading. The tests carried out mainly focussed on the application of tension to reinforced concrete.

The initial single elements tests provided code verification, demonstrating that where displacements localise within zones which are dependent on element length, CDPM2 can provide mesh-independent results.

Once suitable techniques for modelling both plain and reinforced concrete had been established, prisms with varying mesh sizes were analysed. Mesh independency was demonstrated in all analyses of both plain and reinforced concrete. This might provide calculation verification that CDPM2 can provide mesh-independent results for reinforced concrete subjected to axial tension. However, it would be valuable to repeat this investigation for a longer prism to provide more meaningful results (see suggestions for further research below).

Once a suitable method of modelling the reinforced concrete had been established, results were compared to Bischoff's tension stiffening experiment. The agreement between model and experimental results suggests that CDPM2 is capable of producing results which agree well with tension stiffening tests using plain concrete. The results for the fibre-reinforced concrete generally agreed with Bischoff's results. The effect on crack spacing of changes to bond properties was partly captured by the models.

Although these results indicate that CDPM2 is capable of producing results which agree with tension stiffening experiments, it is important to note that shrinkage effects should be considered to provide a proper validation (see suggestions for further research below).

5.2 Suggestions for Further Work

In this project, the small prisms analysed were fairly short. In order to produce cracks, the length of the prisms should be increased to produce more meaningful results.

It would be interesting to model the bond-slip relationship with the method using shared nodes and 'springs' to reflect the strength of the bond between concrete and reinforcement, to see how this affects the results. It might allow the effect of changes in bond properties to be captured better.

More detail could be obtained for the reinforced concrete analyses conducted in this project if the force and/or strain distribution in the reinforcement was plotted at different stages of the analysis. The strain distribution should show the maximum strain at crack locations, reducing away from the crack.

An important improvement to this project would be to include the effects of shrinkage by appropriately altering the responses obtained. This should provide a better agreement between model and experiment responses and therefore provide more reliable results.

This project modelled concentrically reinforced concrete prisms with only one reinforcing bar. It would be interesting to investigate the effect of including more reinforcing bars. Other changes which could be investigated are the use of high strength concrete and the increase of concrete cover around the reinforcement.

This project focussed on loading the reinforced concrete in axial tension. Other areas for investigation are multiaxial tension, both axial and multiaxial compression, and bending.

6 REFERENCES

Bhushan, K. (2010) “What is Quasi-Brittle Fracture and How to Model its Fracture Behaviour”, The FESI Bulletin: International Magazine on Engineering Structural Integrity [Electronic] vol. 4, no. 4, Autumn, p. 18, Available: http://www.fesi.org.uk/fesi bulletins/FESI_bulletin_Autumn_2010_V2.pdf [7 Jan 2017].

Bischoff, P. (2001) “Effects of shrinkage on tension stiffening and cracking in reinforced concrete”, Canadian Journal of Civil Engineering [Electronic], vol. 28, no. 3, pp. 363-374, Available: http://www.nrcresearchpress.com/doi/pdf/10.1139/l00-117 [7 Jan 2017].

Bischoff, P. (2003) “Tension Stiffening and Cracking of Steel Fiber-Reinforced Concrete”, Journal of Materials in Civil Engineering, vol. 15, no. 2, April, pp. 174-182.

Bright, N. and Roberts, J. (2010) “Structural Eurocodes: Extracts from the Structural Eurocodes for Students of Structural Design”, 3rd Edition, London: BSI.

CEB-FIP (1990) “CEB-FIP Model Code 1990: Design Code”, London: Thomas Telford.

CEB-FIP (2010) “CEB-FIP Model Code 2010” fib Bulletin 65, vol.1, pp. 120-125.

Chen, W. (2007) “Plasticity in Reinforced Concrete” J. Ross Publishing, pp. 19-25. (Original work published 1982.)

Fields, K. and Bischoff, P. (2004) “Tension Stiffening and Cracking of High-Strength Reinforced Concrete Tension Members” ACI Structural Journal, vol. 101, no. 4, July-August, pp 447-456.

Fraser, A. (2016) “Bomb-proof structures: Modelling of failure of concrete subjected to dynamic loading using LS-DYNA” MSc Thesis, University of Glasgow, Glasgow, Scotland.

Grassl, P. (2016) “User manual for MAT_CDPM (MAT_273) in LS-DYNA” [Electronic] Available: http://petergrassl.com/Research/DamagePlasticity/CDPMLSDYNA/index.html [7 Jan 2017].

Grassl, P., Xenos, D., Nyström, U., Rempling, R., Gylltoft, K. (2013) “CDPM2: A damage-plasticity approach to modelling the failure of concrete”, International Journal of Solids and Structures, [Electronic] vol. 50, no. 24, pp. 3805-3816. Available: http://www.sciencedirect.com/science/article/pii/S0020768313002886 [7 Jan 2017].

Hillerborg, A., Modéer, M. and Petersson, P-E. (1976) "Analysis of crack formation and crack growth in concrete by means of fracture mechanics and finite elements." Cement and concrete research 6, no. 6, pp. 773-781.

Jirásek, M. and Bazant, Z. (2002) “Inelastic Analysis of Structures”, Wiley.

Livermore Software Technology Corporation (2002) “Getting Started with LS-DYNA” [Electronic] Available: http://www.lstc.com/download/manuals [7 Jan 2017].

Livermore Software Technology Corporation (2006) “LS-DYNA Theory manual” [Electronic] Available: http://www.lstc.com/download/manuals [7 Jan 2017].

Livermore Software Technology Corporation (2016a) “LS-DYNA Keyword User's Manual” [Electronic] vol. 2-Material Models. Available: http://www.lstc.com/download/manuals [5 Oct 2016].

Livermore Software Technology Corporation (2016b) “LS-DYNA Keyword User's Manual” [Electronic] vol. 1. Available: http://www.lstc.com/download/manuals [5 Oct 2016].

McTaggart, S. (2016) “LS-DYNA for Analysing the Failure of Concrete Structures” MEng Thesis, University of Glasgow, Glasgow, Scotland.

Mitchell, D., Abrishami, H., and Mindess, S. (1996) ‘‘The effect of steel fibers and epoxy-coated reinforcement on tension stiffening and cracking of reinforced concrete.’’ ACI Materials Journal, vol. 93, no. 1, pp. 61–68, American Concrete Institute.

Nesset, J. and Skoglund, S. (2007) “Reinforced Concrete Subjected to Restraint Forces”, Master’s Thesis, Chalmers University of Technology, Göteborg, Sweden.

Schaller, C. (ed.), Thacker, B., Doebling, S., Francois, H., Anderson, M., Pepin, J. and Rodriguez, E (2004) “Concepts of Model Verification and Validation”, Los Alamos National Laboratory.

Schwer, L. (2014) “Modeling Rebar: The Forgotten Sister in Reinforced Concrete Modeling”.

Williams, K. (2012) “Civil Engineering Materials 1” p. 2.1, University of Glasgow, Department of Civil Engineering.

7 APPENDICES

7.1 Appendix 1 - Input File for Single Element Test

The following is the input file for the single element subjected to tension, in section 4.1.

```
*KEYWORD
*TITLE
 Simulation of Single Small Brick subjected to tension
$
*Parameter
$---+----1----+----2----+----3----+----4----+----5----+----6----+----7----+----8
r Tstart    0.0     r Tend      10.       r DtMax   100.e-3 r MaxDisp   5.e-4
r TSSFAC    0.8     i LCTM      9         r TconP     30.0
*Parameter_Expression
$
 r TDplot    Tend/8
 r TASCII    TDplot/30.0
$
r Tend2    2.0*Tend
$
$   SOLID ELEMENT TIME HISTORY BLOCKS
*DATABASE_HISTORY_SOLID
 1
$
*PART
$#                                                                          title
boxsolid
$#     pid     secid       mid     eosid      hgid      grav    adpopt      tmid
         1         1         1
$$$$$$$$$$$$$$$$$$$$$$$$$$$$$$$$$$$$$$$$$$$$$$$$$$$$$$$$$$$$$$$$$$$$$$$$$$$$$$$
$                                 CONTROL OPTIONS                               $
$$$$$$$$$$$$$$$$$$$$$$$$$$$$$$$$$$$$$$$$$$$$$$$$$$$$$$$$$$$$$$$$$$$$$$$$$$$$$$$
$---+----1----+----2----+----3----+----4----+----5----+----6----+----7----+----8
*CONTROL_ENERGY
         2         2         2         2
*CONTROL_SHELL
  20.0             1        -1         1         2         2         1
*CONTROL_TIMESTEP
$   DTINIT    TSSFAC      ISDO    TSLIMT     DT2MS      LCTM     ERODE     MS1ST
    0.0000       0.8         0     0.000     0.000     &LCTM
*CONTROL_TERMINATION
   &Tend
*CONTROL_OUTPUT
$  NPOPT NEECHO NREFUP IACCOP OPIFS IPNINT IKEDIT IFLUSH
      1,   3,      ,       ,     ,    50
$$$$$$$$$$$$$$$$$$$$$$$$$$$$$$$$$$$$$$$$$$$$$$$$$$$$$$$$$$$$$$$$$$$$$$$$$$$$$$$
$                                   TIME HISTORY                                $
$$$$$$$$$$$$$$$$$$$$$$$$$$$$$$$$$$$$$$$$$$$$$$$$$$$$$$$$$$$$$$$$$$$$$$$$$$$$$$$
*DATABASE_ELOUT
$       dt
   &TASCII
*DATABASE_GLSTAT
$       dt
   &TASCII
*DATABASE_MATSUM
$       dt
```

```
   &TASCII
*DATABASE_NODFOR
$       dt
   &TASCII
*DATABASE_SPCFORC
$#      dt
   &TASCII
*DATABASE_BINARY_D3PLOT
$       dt
   &TDplot
$
$---+----1----+----2----+----3----+----4----+----5----+----6----+----7----+----8
*DATABASE_EXTENT_BINARY
$    neiph     neips    maxint    strflg    sigflg    epsflg    rltflg    engflg
         5                              1         1         1
$   cmpflg    ieverp    beamip
                   0
$---+----1----+----2----+----3----+----4----+----5----+----6----+----7----+----8
*SECTION_SOLID
$#   secid    elform       aet
         1         1         0
$ Material
*Include
material.k
$$$$$$$$$$$$$$$$$$$$$$$$$$$$$$$$$$$$$$$$$$$$$$$$$$$$$$$$$$$$$$$$$$$$$$$$$$$$$$$
$                                BOUNDARY DEFINITIONS                           $
$$$$$$$$$$$$$$$$$$$$$$$$$$$$$$$$$$$$$$$$$$$$$$$$$$$$$$$$$$$$$$$$$$$$$$$$$$$$$$$
$---+----1----+----2----+----3----+----4----+----5----+----6----+----7----+----8
*Boundary_SPC_NODE
$     NID       CID      DOFX      DOFY      DOFZ     DOFRX     DOFRY     DOFRZ
         1         0         1         1         1         0         0         0
         2         0         0         1         1         0         0         0
         3         0         1         0         1         0         0         0
         4         0         0         0         1         0         0         0
         5         0         1         1         0         0         0         0
         6         0         0         1         0         0         0         0
         7         0         1         0         0         0         0         0
         8         0         0         0         0         0         0         0
*Boundary_Prescribed_Motion_Set
$       ID       DOF       VAD      LCID        SF       VID     DEATH     BIRTH
         1         3         2       111       1.0
$ applied z-direction displacement
*DEFINE_CURVE
 111, 0, 1., 1., 0., 0.
  0.0,     0.0
  &Tend,   &MaxDisp
  &Tend2,  &MaxDisp
$ maximum time increment
*DEFINE_CURVE
9,0,1.,1.,0.,0.
   0.0,  &DtMax
 &Tend,  &DtMax
 &Tend2, &DtMax
$
*Include
element.k
*END
```

The same file was used for compression, with `MaxDisp = -5.e-3`

7.2 Appendix 2 - Input File for Small Prism

The same file was used for the plain small prism, in section 4.2, as for the single element in tension, with different part and set IDs and the following alterations:

`MaxDisp = 5.e-4` (`5.e-5` for slow analysis; `5.e-3` for fast analysis)

`TDplot = Tend/50` for fast analysis

`elform = 10.`

Boundary definitions were as follows:

```
$---+----1----+----2----+----3----+----4----+----5----+----6----+----7----+----8
*Boundary_Prescribed_Motion_Set
$       ID       DOF       VAD      LCID        SF       VID     DEATH     BIRTH
         2         3         2       111       1.0
*BOUNDARY_SPC_SET
$       ID       CID      DOFX      DOFY      DOFZ     DOFRX     DOFRY     DOFRZ
         1         0         0         0         1
*BOUNDARY_SPC_SET
$       ID       CID      DOFX      DOFY      DOFZ     DOFRX     DOFRY     DOFRZ
         3         0         1         1         1
*BOUNDARY_SPC_SET
$       ID       CID      DOFX      DOFY      DOFZ     DOFRX     DOFRY     DOFRZ
         4         0         0         1         1
```

The same file was used for the reinforced small prism as for the single element in tension, with different part and set IDs and the following alterations:

`elform = 10.`

Reinforcement was included as follows:

```
$---+----1----+----2----+----3----+----4----+----5----+----6----+----7----+----8
*PART
reinforcement
$      pid     secid       mid     eosid      hgid      grav    adpopt      tmid
        13         1         1         0         0         0         0         0
*SECTION_BEAM_TITLE
Section reinforcement
$#   secid    elform      shrf   qr/irid       cst     scoor       nsm
         1         1       1.0         2         1       0.0       0.0
$#     ts1       ts2       tt1       tt2     nsloc     ntloc
     0.020     0.020       0.0       0.0       0.0       0.0
```

Boundary definitions for the prism with the whole top face loaded were the same as for the plain small prism (above). For the prism with only the reinforcement loaded, the boundary definitions were as follows:

```
$---+----1----+----2----+----3----+----4----+----5----+----6----+----7----+----8
*BOUNDARY_SPC_SET
$       ID       CID      DOFX      DOFY      DOFZ     DOFRX     DOFRY     DOFRZ
         4         0         1         1         1                             1
```

The constrained nodes prism with perfect bond included the following:

```
$---+----1----+----2----+----3----+----4----+----5----+----6----+----7----+----8
*CONSTRAINED_BEAM_IN_SOLID
$        |         |         |         |         |         |         |         |
$    slave    master     sstyp     mstyp                           nquad      cdir
        13         1         1         1                                       0
$        |         |         |         |         |         |         |         |
$    start       end               axfor
        0.        0.                  0.
```

The constrained nodes prism with bond-slip included the following:

```
CONSTRAINED_BEAM_IN_SOLID
$---+----1----+----2----+----3----+----4----+----5----+----6----+----7----+----8
$        |         |         |         |         |         |         |         |
$    slave    master     sstyp     mstyp                           nquad      cdir
        13         1         1         1                                       1
$        |         |         |         |         |         |         |         |
$    start       end               axfor
        0.        0.                -10
*DEFINE_FUNCTION
$        |         |         |         |         |         |         |         |
        10
float force(float slip,float leng)
{
float force,pi,d,area,shear,pf,s1,s2,s3,tmax,tf;
pi = 3.1415926;
d = 0.016;
s1 = 0.6e-3;
tmax = 8e6;
area = pi*d*leng;
if(slip < s1) {
shear = tmax*(slip/s1)**0.4;
} else{
shear = tmax;
}

force = shear*area;
return force;
}
```

7.3 Appendix 3 - Input File for Tension Stiffening Test Prism

The same file was used for the tension stiffening test prisms, in section 4.3, with perfect bond using shared nodes; perfect bond using constrained nodes; and bond-slip using constrained nodes as for the respective small reinforced prisms, with different part and set IDs and the following alterations:

```
MaxDisp = 2.5e-3
TDplot = Tend/20
```

The diameter of the reinforcement was increased as follows:

```
*SECTION_BEAM_TITLE
Section reinforcement
$#   secid    elform      shrf   qr/irid       cst     scoor       nsm
         1         1       1.0         2         1       0.0       0.0
$#     ts1       ts2       tt1       tt2     nsloc     ntloc
     0.016     0.016       0.0       0.0       0.0       0.0
```

The ends of the reinforcement were thickened by including the following:

```
*PART
reinforcement
$      pid     secid       mid     eosid      hgid      grav    adpopt      tmid
        14         3         1         0         0         0         0         0
*SECTION_BEAM_TITLE
Section reinforcement
$#   secid    elform      shrf   qr/irid       cst     scoor       nsm
         3         1       1.0         2         1       0.0       0.0
$#     ts1       ts2       tt1       tt2     nsloc     ntloc
    0.0195    0.0195       0.0       0.0       0.0       0.0
```

For the prisms with bond-slip, the maximum bond stress was initially changed to `tmax = 14.8e6` and this was altered as outlined in section 4.3.2.